

Building Digital Societies as Ecosystems: How Recognition and Repeat Relationships Sustain Cross-Community Work in Open Source

Lucia Gomez Tejeiro^{1,2†}, Thibaut Chataing¹,
Julian Jang-Jaccard³, Alain Mermoud³, Thomas Maillart^{1*†}

^{1*}Geneva School of Economics and Management, University of Geneva,
Bvd. Pont-d'Arve, 40, Geneva, 1205, Switzerland.

²Institute for Applied Data Science and Finance, Bern University of
Applied Sciences, Brückenstrasse 73, Bern, 3012, Switzerland.

³armasuisse Science and Technology, EPFL Innovation Park, Bâtiment
I, Lausanne, 1015, Switzerland.

*Corresponding author(s). E-mail(s): thomas.maillart@unige.ch;
Contributing authors: lucia.gomez@unige.ch; thibaut.chataing@unige.ch;
julian.jang-jaccard@armasuisse.ch; alain.mermoud@armasuisse.ch;

†These authors contributed equally to this work.

Abstract

We measure cross-boundary collaboration in an open-source software (OSS) ecosystem by reconstructing the bipartite contributor–repository graph of 464 cybersecurity-focused projects and 11,372 contributors active over October 2001–May 2022 (Rawsec Cybersecurity Inventory). Louvain community detection identifies 163 non-singleton communities; per-community contributor count scales superlinearly with repository count ($n_{\text{contributors}} \sim n_{\text{repos}}^{1.4}$), and community formation follows a logistic trajectory saturating around 2018. Three patterns support a recognition / repeat-relationship account of cross-boundary work. *First*, cross-community work concentrates in a thin *carrier layer*: only nine canonical humans span seven or more communities at the commit level, authoring 14% of 4,015 inter-community merged pull-requests; the top-50 cross-community contributors produce 54%. *Second*, boundary friction is a recognition cost, not a fixed boundary property: inter-community pull-request acceptance rises

from 42% at breadth $k = 1$ to 87% at $k = 5-9$, with median latency compressing from 147 h to 49 h. *Third*, community survival is cohort-structured: per-cohort residualisation hazard rises an order of magnitude between pre-2010 and 2018 cohorts, and external community reach predicts survival mainly through community size, leaving late-cohort communities under-served despite a stable carrier layer. The corpus predates mainstream LLM coding assistants; this baseline of carrier-layer thinness, friction gradient, and cohort hazard informs debates on *social coding* as a template for digital societies and on what AI-mediated OSS ecosystems should not optimise away.

1 Introduction

Open source software (OSS) has moved from economic oddity [1] to load-bearing infrastructure: encryption libraries, security tooling, build systems, and operating-system components are now produced and maintained as OSS [2], and the digital systems that depend on them increasingly mediate physical infrastructures and public services [3–5]. The governance template – bottom-up peer production [6] under permissive licensing [7] – has proven robust enough to scale into the mainstream [8], but the same expansion has made the question of *ecosystem* sustainability concrete: many projects are abandoned or under-maintained [9, 10], and complex dependency networks transmit fragility across organisational boundaries [11]. This raises a focused, measurable question: what holds an OSS ecosystem together when individual projects come and go? The answer matters beyond software, because OSS-like codes and processes already structure live coding for music [12, 13], peer production on Wikipedia [14, 15], and the AI-driven reshaping of scientific discovery itself [16, 17], while increasingly mediating physical systems from urban mobility [18] to energy grids [19] and civic platforms [20]. Cybersecurity, the domain of the ecosystem under scrutiny here, is itself produced and coordinated through these same peer-production processes – from collective vulnerability discovery and open threat-intelligence sharing to the maintenance of critical encryption and security tooling [21–23].

It is well established that contribution *within* OSS projects is heavy-tailed: a small core absorbs most of the integration and quality-control work while a long tail contributes occasionally [24–26], with productive bursts that match self-organised-criticality signatures [27, 28]. This intra-project picture has been extensively documented and is not in dispute. What has received much less ecosystem-scale attention is the *inter*-project layer: the contributors whose commits and pull requests reach across community boundaries, link otherwise loosely coupled projects, and absorb the coordination cost of doing so. Boundary-crossing work is known to be more contested in peer-produced systems – higher review scrutiny, lower acceptance, longer deliberation [29–32] – yet ecosystem-scale evidence on *who* sustains it, and on what such carriers can and cannot do for the communities they bridge, remains thin.

We test how a cybersecurity OSS ecosystem is *born*, *develops*, and is *sustained* by a thin upper tail of cross-community contributors – the nine canonical humans whose commit-level breadth k (the number of distinct Louvain communities they touch) reaches $k \geq 7$, the data-driven inflection of the two-regime fit on the empirical breadth

distribution – and show that this *carrier layer*, while necessary, is not sufficient: a substantial share of communities currently lack any active cross-community contributor, and late-born cohorts enter the residual phase at sharply higher annual hazard than earlier ones. On the bipartite contributor–repository graph of the Rawsec Cybersecurity Inventory (October 2001–May 2022; 11,372 contributors, 464 repositories, 163 non-singleton communities), community formation traces from the pre-GitHub era through the post-2008 acceleration to a logistic-saturation plateau around 2017–2018. At the boundaries, 90.8% of canonical humans commit to a single community and only the nine carrier-layer humans span seven or more; the broader population that ever authors a merged inter-community pull-request is itself a minority (883 canonical humans, 8.4% of the total), and within it the top 50 contributors alone produce 54% of all 4,015 inter-community merged pull-requests. Commit-level breadth and cross-boundary pull-request activity are nearly perfectly rank-ordered across canonical humans (Spearman $\rho = 0.96$), so the carrier layer identified at the commit scale and the contributors who absorb most of the inter-community pull-request volume are essentially the same individuals. Stratifying five depth indicators – acceptance, integration latency, review-state mix, issue deliberation, contributor retention – by contributor breadth k reveals a *recognition premium*: high-breadth contributors clear inter-community PRs at near-intra-community speed and acceptance, while one-off submissions face a 20.8-percentage-point gap and 2–4 \times slower integration. Yet 52% of communities currently host no active cross-community contributor at any breadth, and the per-cohort residualisation hazard rises an order of magnitude for communities born after ~ 2017 . We call the resulting pattern *friction with stable trust*: the ecosystem is workable because the thin upper-tail carrier layer makes boundary-crossing cheap when present, and visibly fragile where it is absent.

The remainder of the paper is organised as follows. Section 2 reviews complex-adaptive-systems and peer-production foundations and motivates the breadth/depth distinction. Section 3 details the Rawsec corpus, identity canonicalisation, the bipartite community detection, and the GitHub Archive enrichment used to build the depth indicators. Section 4 presents (i) community-scale anatomy and core–periphery structure, (ii) the heavy-tailed contributor breadth distribution and its cross-community carrier layer, (iii) community survival and the cohort hazard, and (iv) the boundary-friction depth panel and recognition mechanism. Section 5 situates the findings as a recognition / repeat-relationship account of sustained cross-boundary work and outlines what this implies for the governance of OSS-like ecosystems.

2 Background

OSS ecosystems share with biological, social, and technological complex adaptive systems a small set of organising features: decentralised control, nonlinear interaction, and emergent structure across scales [33, 34]. Two ideas anchor the present study. The first is Holling’s distinction between optimisation and *resilience* – the capacity of a system to absorb disturbance and reorganise rather than maintain a fixed point [35]. The second is Simon’s argument that hierarchical, near-decomposable structure is what lets complex systems evolve and persist [36]. Read together, they frame the question

this paper makes measurable: an OSS ecosystem is workable not when its boundaries are erased but when boundary-spanning structures absorb the perturbations that an explicitly modular system would otherwise transmit.

At the network level, the structural features that shape both robustness and vulnerability are well established: heterogeneous degree distributions, community structure, and core-periphery organisation. Heavy-tailed affiliation arises naturally from multiplicative stochastic growth, in which prior advantage compounds into further attention – the Matthew effect of cumulative advantage [28, 37, 38]. Such systems are robust to random failure but fragile under targeted disruption [39], a “robust-yet-fragile” regime formalised by the Highly Optimized Tolerance framework [40] and observable as far afield as the Internet backbone [41]. Self-organised-criticality dynamics complement this picture by showing that punctuated, cascade-like activity is the norm rather than the exception in evolving networks [27, 42], with hierarchical branching processes providing a generative account of how local interactions cascade into observed bursty, multi-scale activity patterns [43].

OSS communities exhibit these dynamics directly. Production is bursty, contribution is heavy-tailed, and a small core handles integration and quality control while a long tail contributes occasionally [24, 27, 28]. Concentration is a productivity feature rather than a sign of weakness: super-linear scaling between team size and output is documented on platforms as varied as GitHub and Wikipedia [44–46], and the temporal organisation of bursts – short windows of intense, coordinated activity – lets communities respond to emerging needs without sustaining permanent overhead [47]. At the ecosystem scale, the relevant unit of decomposition is *community modularity* – the natural partition of the contributor-repository network into densely connected, weakly coupled groups recovered by network-detection methods [48, 49]. This network-level modularity lets parallel work proceed across many projects with minimal coordination, while the inter-community ties through which knowledge and trust travel define where that parallelism breaks down. Peer-production governance [6] provides the matching social layer, allowing authority to accrue meritocratically through contribution rather than hierarchy. Throughout the rest of this paper, *community* refers to a Louvain community of contributors and repositories on the bipartite graph – the network-detection sense of modularity – and not to a code module or library dependency.

What sustains an OSS ecosystem at the scale of many such communities is the comparatively under-studied question of who and what carries collaboration *across* community boundaries. Sustained engagement and the presence of cross-community contributors have long been associated with knowledge recombination and adaptability in collaborative innovation systems [50, 51], and the keystone-contributor analogy to ecological systems is well-supported on OSS data [44, 45]. Boundary work, however, is not free. Comparative evidence from Wikipedia treats talk-page activity and revert rates as visible traces of coordination cost, showing that cross-boundary edits face higher scrutiny and survive less often than within-group edits [29, 30]. In GitHub code review, Tsay et al. show that social signals – prior contribution history, community membership – shape whether a pull request is accepted, revised, or rejected [31], and Halfaker et al. link concentrated rejections of newcomer contributions to later

attrition [32]. These threads motivate a structured pair of measurement strategies we adopt jointly here: a *breadth* view – how many cross-community links exist and how dense they are – and a *depth* view operationalised through five indicators – pull-request acceptance, integration latency, review-state mix, issue-comment depth, and contributor retention after boundary crossings – so that ecosystem-scale traces speak to whether boundary-spanning collaboration is contested, sustained, and costly, not just whether it occurs.

3 Methods

3.1 Data and contributor identity

We collected GitHub commit, pull-request, and issue activity for the 464 repositories listed under the cybersecurity domain in Rawsec’s Cybersecurity Inventory (RCI) as of May 2022,¹ produced by 11,372 contributors over October 2001–May 2022. The RCI is a curated inventory of state-of-the-art open-source cybersecurity software: projects are listed because they cover a recognised cybersecurity capability (scanning, exploitation, forensics, threat-intelligence sharing, and so on), not because they share a software-functional dependency. There is, a priori, no expectation that one listed project depends on another in the sense of a package-dependency graph; the corpus is therefore not a software ecosystem in the dependency-network sense [11], but an *ecosystem of specialisation* in contributing to open-source cybersecurity software, in which contributors and repositories interact across thematic boundaries through shared maintainers, cross-project pull-requests, and issue-level deliberation rather than through code-level coupling. Two complementary streams support the analyses. The first, collected through the GitHub REST API, retains 214,930 *merged* pull-requests (`state=closed` with non-null `merged_at`) and 602,102 commit records with creation/merge timestamps, user identities, and event types.

GitHub Archive enrichment for collaboration-depth indicators.

The second stream, drawn from the GitHub Archive (<https://www.gharchive.org>) via Google BigQuery for February 2011–May 2022, adds every pull-request, review, and issue event in the same window – including rejected and abandoned PRs (`state=closed`, `merged_at=null`), review states (`APPROVED`, `CHANGES_REQUESTED`, `COMMENTED`, `DISMISSED`), and issue-level activity. The two streams support both the intra- versus inter-community collaboration ratios used at the community scale and the five collaboration-depth indicators reported in Section 4.5: pull-request acceptance rate, integration latency, review-state mix (share of merged PRs receiving at least one `CHANGES_REQUESTED` review), issue discussion depth, and contributor retention after a boundary crossing. Each indicator is stratified by whether the actor’s home (modal) community matches the recipient repository’s community, in line with the comparative literature on cross-boundary coordination cost in peer production [29–32].

¹Rawsec’s Cybersecurity Inventory <https://inventory.raw.pm/tools.html>

The commit metadata uses a numeric `author_uniqueID` in 86.9% of rows; the GitHub Archive stream uses login strings throughout. We canonicalise contributor identity via an `actor_id` \leftrightarrow `actor_login` map built from the GitHub Archive (490,990 `actor_ids`, 507,395 logins), then exclude 11 explicit bots (logins matching `*[bot]` or on a curated automation list) and 688 phantom git identities (numeric IDs that do not resolve to a login plus the generic placeholders `root/admin/git/user`), leaving 10,490 canonical human contributors on which all cross-community contributor analyses are computed. Repository sample-construction details (renaming preservation, technology annotation), the full bot/phantom list, and the per- k filter sensitivity analysis are documented in Supplementary S.8.1.

3.2 Bipartite community detection

We model the data as a weighted bipartite graph $G = (U, V, E)$ with contributor nodes U , repository nodes V , and edges of weight $\log(1 + c)$ where c is the per-pair commit count, in line with prior bipartite-affiliation measurement of cooperation structures in peer production [15]. Louvain community detection (`igraph` implementation, resolution = 0.5) on this weighted bipartite graph yields 163 non-singleton contributor–repository communities. Per community c we compute intra- and inter-community link densities and their ratio (rescaled to $[0, 1]$ for plotting), the contributor-/repository-heavy size coordinates ($|U_c|, |V_c|$), and the inter-community PR share. At the contributor scale we use the participation breadth k_i – the number of distinct Louvain communities contributor i touches at the commit level – and treat the upper-tail population $k_i \geq 7$ identified by the data-driven two-regime fit of Figure 3C (Supplementary S.5.1) as the boundary-spanning carrier layer used throughout the Results. The bipartite graph is the natural object of inference here because community-scale structure is not recoverable from one-mode projections of G , which inflate degree and discard the asymmetry between occasional co-presence and sustained co-affiliation [52, 53]; the projection-versus-bipartite diagnostic (ARI/NMI/purity/-Jaccard) is reported in Supplementary S.1. Throughout, *community* denotes a Louvain community of contributors and repositories on the bipartite graph and not a code module or library dependency.

3.3 Temporal dynamics

At the ecosystem scale we compute yearly *inflection scores* – the relative change in total commit counts between consecutive years – and Gaussian-kernel-smooth them to expose periods of acceleration, deceleration, or stasis (Figure 1A). At the community scale we summarise each non-singleton Louvain community by its vector of annual commit totals and visualise the per-community trajectories as a temporal heatmap sorted by birth year (Figure 2A); an exploratory unsupervised clustering of these trajectories using a Seurat-style log-normalisation + PCA + UMAP + Louvain pipeline [54] is reported in Supplementary S.3.2 and used only as an exploratory device. We additionally fit a three-parameter logistic to the cumulative-births series $N_{\text{born}}(y)$ and decompose the ecosystem-wide annual commit total $T(y)$ multiplicatively into an extensive margin (active-community count $N(y)$) and an

intensive margin (mean commits per active community $\bar{e}(y) = T(y)/N(y)$) following the Kaya-identity decomposition tradition [55, 56]; the resulting log-additive identity $\Delta \log T = \Delta \log N + \Delta \log \bar{e}$ and the regime-mean decomposition are reported in Supplementary S.3.1.

3.4 Community survival analysis

To characterise community survival we treat the residual phase as a right-censored time-to-event outcome. For each non-singleton community c with annual commit series $a_c(y)$ over $y \in [b_c, Y_{\text{end}}]$, where $b_c = \min\{y : a_c(y) > 0\}$ is the birth year and $Y_{\text{end}} = 2021$ is the last full year of GitHub Archive coverage, let μ_c be the mean yearly activity over that span and $\theta_c = 0.05 \mu_c$ a residual threshold. The last non-residual year is $y_c^* = \max\{y \in [b_c, Y_{\text{end}}] : a_c(y) \geq \theta_c\}$; the non-residual span is $y_c^* - b_c + 1$ years; communities with $y_c^* = Y_{\text{end}}$ are right-censored. Across the 163 non-singleton communities, 55 enter residual by 2021 and 108 are censored. We summarise the cohort dependence as the per-cohort annual hazard

$$h(\text{cohort}) = \frac{\#\{\text{events in cohort}\}}{\sum_{c \in \text{cohort}} (y_c^* - b_c + 1)}, \quad (1)$$

which normalises by years-at-risk and is therefore not mechanically driven by the geometric censoring envelope $Y_{\text{end}} - b_c + 1$. We then test whether cross-community connectivity is associated with survival in two complementary ways. First, Kaplan–Meier non-residual probability is estimated separately on tertiles of (i) the inter-community PR share and (ii) $\log_{10}(1 + d_c^{\text{ext}})$, where d_c^{ext} is the symmetric number of other communities c exchanges commits with, and the curves are compared with multi-group log-rank tests. Second, a multivariate Cox proportional-hazards model (`lifelines.CoxPHFitter`) regresses time-to-residual on the same connectivity covariates while controlling for cohort (birth year) and size (\log_{10} # repositories, \log_{10} # contributors). Threshold sensitivity (1%, 5%, 10% of mean yearly), the full univariate and multivariate Cox specifications, and the static-window/reverse-causation caveats are documented in Supplementary S.7.1 and Supplementary S.7.2.

3.5 Predictive forecasting of repository activity

To test whether community-level structural features carry predictive content for repository activity beyond short-run autocorrelation, we trained two Random Forest regressions of six-month commit volume per repository (`randomForest` in R) – one with and one without the previous six months of commits as a feature – and ranked features by the percentage increase in mean square error (MSE) under permutation. Inputs comprised contributor-subtype indicators, cumulative commit activity and repository age, event-ratio scores, accumulated PR counts, repository-level inter-to-intra link-density summaries, community membership labels, the number of inter-community links, and clustering annotations. The full ablation comparison and prediction-error scatters are reported in Supplementary S.6.

4 Results

The reconstructed bipartite network of contributor–repository interactions, aggregated from October 2001 to May 2022, comprises 11,372 contributors and 464 repositories drawn from the Rawsec Cybersecurity Inventory. Edges represent at least one commit event and are weighted by interaction frequency. Louvain community detection on this weighted bipartite graph identifies 163 non-singleton contributor–repository communities, varying in internal cohesion and cross-community coupling. The structural transformation of the ecosystem across three representative snapshots (2005, 2008, 2017) of the bipartite contributor–repository graph and the corresponding longitudinal network-level metrics are summarised in Figure 1. Figure 2 then characterises these 163 communities at the community level: their temporal development across the observation window (panel A) and the joint distribution of repositories and contributors per community in the heavy-tailed plane (panel B).

4.1 Community structure and cross-community coupling

The structural analysis reveals that the OSS cybersecurity ecosystem exhibits a highly skewed distribution of contributor–repository associations, with a small number of communities accounting for a large share of contributors or repositories. Quantifying this skew across the 163 non-singleton Louvain communities, the Gini coefficients of the distributions of contributor counts and repository counts per community are approximately 0.80 and 0.57, respectively (median community size: 4 contributors and 1 repository; 90th percentile: 109 contributors and 7 repositories). For example, community 2 comprises 868 contributors and 14 repositories, community 74 comprises 502 contributors and 3 repositories, and community 17 comprises 235 contributors and 50 repositories, illustrating **contributor-heavy** versus **repository-heavy** community extremes in the community–size plane (Figure 2B). The contributor-heavy communities such as 2 and 74 that combine many active contributors with relatively few repositories sit toward the upper range of inter-to-intra link-density ratios, while smaller and less active communities are largely localised within their own boundaries. Across the 124 multi-contributor communities, contributor count scales superlinearly with repository count: an OLS fit in log–log space gives $n_{\text{contributors}} \sim n_{\text{repos}}^\beta$ with $\beta = 1.4(1)$ ($R^2 = 0.64$, $p < 10^{-3}$), so communities accrue contributors faster than they accrue repositories and the largest communities sit well above a constant-team-size line. These labels refer to community-scale affiliation imbalance, not to unipartite degree or eigenvector centrality among individuals; the community-scale structure reported here is not recoverable from one-mode projections of the bipartite graph, which systematically inflate degree and blur fine structure (Supplementary Figure S3). Commit activity is positively associated with cross-community coupling at the community scale – a Spearman rank correlation of $\rho \approx 0.75$ ($p < 10^{-3}$) between per-community total commits and the rescaled inter-to-intra link-density ratio (Supplementary Figure S6) – consistent with prior research on modular software architecture and productivity in OSS ecosystems [57]. The exponent $\beta = 1.4(1) \approx 4/3$ places this community-scale measurement squarely within the superlinear team-size-to-productivity scaling reported on individual OSS projects, a well-documented regime

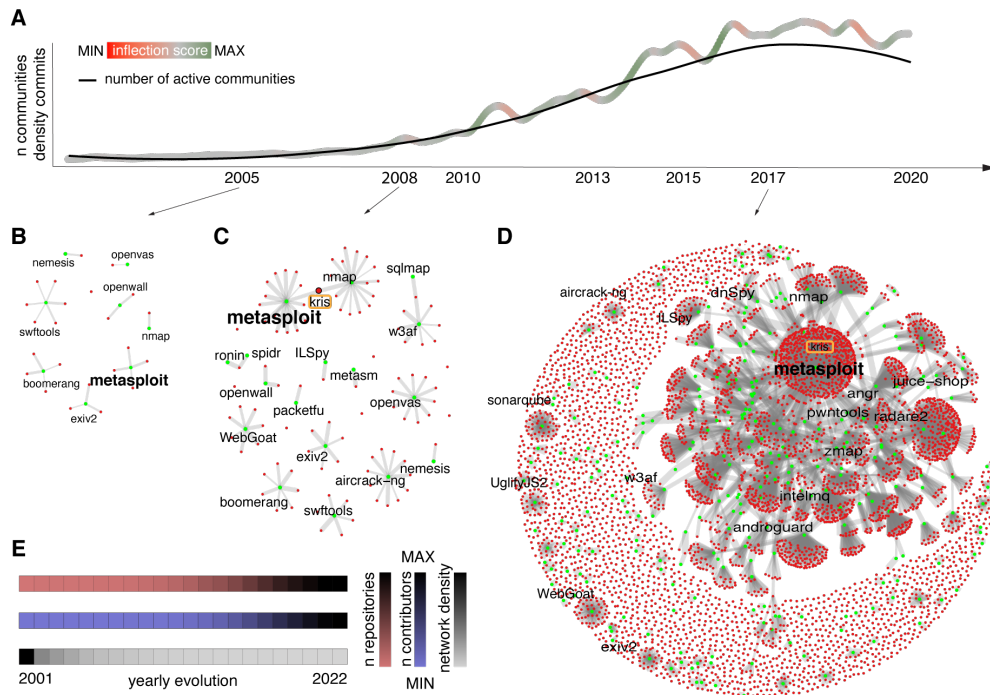


Fig. 1 Bipartite contributor–repository graph: ecosystem-level activity, representative snapshots, and longitudinal metrics. **A.** LOESS curve fit on the number of communities through time (black line) overlaid on a Gaussian kernel density of commit activity colour-coded by the inflection score (point-to-point differential): red (negative inflection), grey (neutral), green (positive); positive peaks correspond to surges in network-wide development activity. **B.** Commit-activity bipartite network snapshot at the end of 2005 (contributors in red, repositories in green, grey edges weighted by commit counts). **C.** Snapshot at the end of 2008: one contributor (*kris*, highlighted in orange) marks the onset of measurable cross-repository ties, coinciding with the official launch of GitHub on April 10, 2008. **D.** Snapshot at the end of 2017: the ecosystem has settled into a dense community-scale core–periphery layout, with *metasploit* (initially linked to *nmap* by *kris* in 2008) standing out as a highly affiliated repository among interconnected contributor groups. **E.** Stack of heatmaps tracking three network-level metrics over time: number of repositories (gradient: low (red) – high (black)), number of contributors (low (blue) – high (black)) and global network density (low (grey) – high (black)); the per-community equivalent of the activity timeline appears in Figure 2A.

in which the whole production is more than the sum of its parts, through critical cascades of contributions[44, 45]. Our result extends that within-team superlinearity by one level of aggregation: at the community scale, bigger repository portfolios attract disproportionately more contributors, as the same coordination dynamics that make larger OSS teams individually more productive also recruit them at higher rates, possibly offering diversified opportunities for joining and specialisation in a more modular community organisation [58].

Together these features delineate a pronounced *community-scale* core–periphery pattern in which high-coupling, high-activity communities may act as engines of collaboration and knowledge flow as well as potential points of systemic fragility.

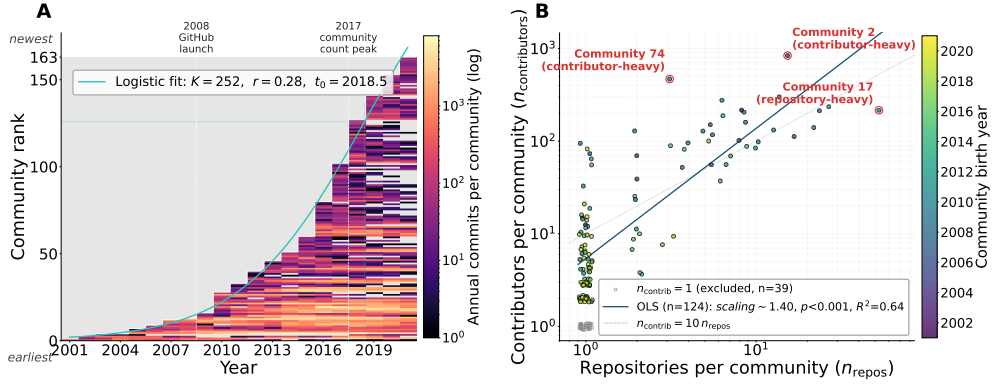


Fig. 2 Anatomy of communities: temporal development and size scaling. **A.** Annual commits per community on a log colour scale (rows = 163 non-singleton Louvain communities sorted by birth year, columns = years 2001–2022; light grey cells are pre-birth or zero-activity years). The white step traces the empirical cumulative number of communities born by each year; the cyan curve is a logistic fit (parameters in main text). White dashed verticals mark the GitHub launch (April 2008) and the fitted inflection year t_0 . **B.** Per-community joint distribution in the $(n_{\text{repos}}, n_{\text{contributors}})$ plane on log–log axes. Filled markers (viridis by community birth year, sharing the year axis of panel A) are the $n = 124$ communities with $n_{\text{contributors}} > 1$ that enter the OLS power-law fit (blue line; parameters in main text); the 39 single-contributor communities are shown as small open grey markers and excluded from the fit (justification in Supplementary S.2.1). The dotted diagonal marks $n_{\text{contributors}} = 10 n_{\text{repos}}$. Communities 2, 74 (contributor-heavy) and 17 (repository-heavy), cited in the text, are circled in red.

4.2 Temporal Evolution of the OSS Ecosystem

The temporal trajectory of community formation and commit activity in the RCI ecosystem from 2001 to 2022 reveals a sustained increase in the number of active communities through a peak in 2017, followed by a plateau. A LOESS-smoothed curve tracking the number of communities over time (Figure 1A) delineates three distinct phases: a period of gradual expansion (2001–2007), a phase of rapid growth (2008–2014), and a slower expansion approaching saturation (2015–2017); the overlaid Gaussian kernel density of commit activity, colour-coded by inflection score, highlights alternating periods of acceleration (green) and contraction (red). The structural transformation of the ecosystem is visualised at the bipartite-graph level in Figure 1B–D: in 2005, prior to the emergence of GitHub, the network comprises small, disconnected communities with limited contributor overlap; by 2008, following the official launch of GitHub on April 10, 2008, structural cohesion increases and the first bridging contributor (*kris*) emerges, marking the onset of measurable cross-community ties; by 2017, the ecosystem exhibits a dense community-scale core–periphery layout, with *metasploit* – initially linked to *nmap* by *kris* in 2008 – standing out as a highly affiliated repository.

Longitudinal heatmaps tracking network-level metrics (Figure 1E) show that while the number of repositories and contributors grows steadily, overall network density peaks early and then declines sharply. This decline reflects a scaling effect, whereby the addition of new nodes and links does not fully compensate for the dilution of global graph density. Structurally, this reflects a shift toward decentralised collaboration and increasing community specialisation, with growth driven more by the formation of

new clusters than by the expansion of existing, tightly coupled core communities. This decentralisation–specialisation dynamic marks a transition from a highly integrated growth phase toward a more federated, domain-focused organisational structure. The same three regimes are visible at the per-community level in the temporal heatmap of Figure 2A, which exposes substantial heterogeneity in when individual communities are born, peak, and decline within the observation window. We model the empirical cumulative count of community births $N(t)$ with the canonical Verhulst logistic equation [59] – the standard model for growth bounded by a finite carrying capacity, in which the per-capita growth rate decreases linearly with current size,

$$\frac{dN}{dt} = rN\left(1 - \frac{N}{K}\right), \quad N(t) = \frac{K}{1 + e^{-r(t-t_0)}}, \quad (2)$$

where K is the carrying capacity, r the intrinsic growth rate, and t_0 the inflection year. The model is appropriate here because the niche the corpus indexes – canonical OSS cybersecurity capabilities (scanning, exploitation, forensics, threat-intelligence sharing, ...) – is itself bounded: once the recognised capability space is largely filled, new communities form less frequently, and the cumulative-births trajectory necessarily saturates. Fitting Equation (2) to the empirical cumulative-births series over the full calendar years 2001–2021 (Figure 2A, white step / cyan curve; the partial-year 2022 is excluded for consistency) returns $K = 252 \pm 27$ communities, $r = 0.28 \pm 0.02 \text{ yr}^{-1}$, and $t_0 = 2018.5 \pm 0.8$, quantifying the saturation visible in the cumulative trajectory. A multiplicative decomposition of ecosystem-wide annual commits into an extensive margin (active-community count N) and an intensive margin (mean commits per active community \bar{e}) shows that mean per-community intensity peaked four years earlier, in 2014, before N began to saturate – the aggregate masked the per-community decline for ~ 4 years (Supplementary S.3.1).

These temporal patterns display *at once* the vigour of the OSS cybersecurity ecosystem of communities and the seeds of its fragility. The vigour is visible in the trajectory itself: a roughly two-decade run from a handful of disconnected communities pre-GitHub to a dense, broadly cohesive bipartite graph by 2017, with cumulative community births well-fit by a single logistic growth law – a clean signature of an ecosystem whose niche of recognised cybersecurity capabilities was being rapidly populated under the institutional shift to GitHub. The fragility is built into the same trajectory: the carrying capacity K is finite by construction, the births inflection has already passed ($t_0 \approx 2018.5$), and the multiplicative decomposition shows that the intensive margin – mean commits per active community – had already started to fall in 2014, four years before the extensive margin saturated, so the headline ecosystem-wide commit total was sustained for half a decade by an inflow of new communities that masked an internal slowdown invisible to aggregate metrics. The cohort hazard developed in Section 4.4 sharpens the same point quantitatively: communities born after the count-peak transition are intrinsically more residualisation-prone, so the same maturation that produced the ecosystem’s vigorous growth phase is also the dynamic by which it has begun to encode its own structural exposure.

The implication for the rest of this section is direct. Once the extensive margin has saturated and the per-community intensive margin has begun to thin, what sustains

a matured ecosystem of 163 non-singleton communities is no longer the inflow of new communities but whatever *cross-community* structure links the existing ones to each other. The next subsection examines that structure at two scales – community-scale heterogeneity in intra/inter pull-request activity and contributor-scale concentration of community-spanning commits – before the survival analysis (Section 4.4) and boundary-friction stratification (Section 4.5) quantify the consequences.

4.3 Cross-Community Collaboration and Structural Drivers of Activity

Following the maturation picture above, we ask how collaboration extends across the boundaries between the 163 non-singleton communities once the ecosystem stops being driven by the inflow of new ones. We examine that question at two scales: pull-request activity at the community level (Figure 3A–B) and the underlying contributor-level commit pattern that supports it (Figure 3C–D). A heatmap and dendrogram of intra-versus inter-community pull-request ratios (Figure 3A) reveal strong heterogeneity in collaborative behaviour: some communities remain highly inward-focused, while others resolve a substantial portion of development issues across community lines. These more outward-oriented communities cluster together, and their collaborative capacity correlates with community size, contributor engagement, and the presence of cross-community contributors (Figure 3B). These patterns reinforce prior findings that sustained engagement and cross-boundary collaboration are central to distributed innovation systems and community productivity [58, 60].

The community-level breadth signal observed in Figure 3A–B is supported, at the contributor scale, by a sharply heavy-tailed distribution of community participation (Figure 3C): of the 10,490 canonical human contributors that remain after canonicalising identity and removing 11 bots and 688 phantom git identities (Methods Section 3.1), 9,524 (90.8%) commit only inside a single community, 966 (9.2%) cross at least one boundary at the commit level, only 43 (0.4%) span five or more distinct communities, 9 (0.09%) span seven or more, and the most-spanning contributor reaches $k = 30$. The empirical probability mass function (PMF), smoothed by an adaptive Abramson kernel-density estimate (KDE) on $\log_{10} k$, has a two-regime structure with a data-driven inflection at $k^* = 7$, selected by minimising the body+tail OLS sum of squared residuals (SSR) over candidate transitions (Supplementary S.5.1). Calibrating straight lines on double-logarithmic axes recovers, for the body ($k < 7$), a single power-law regime with PMF slope $\alpha = 3.73$ – equivalently a complementary CDF (CCDF) exponent $\mu = \alpha - 1 = 2.73$; with $\mu > 2$ the body is *not* heavy-tailed in the standard sense (finite mean and finite variance). The tail ($k \geq 7$, nine humans) is by contrast essentially flat in log–log space (slope -0.61): probability is very nearly constant across the upper tail rather than continuing the body’s rapid decay. The six-fold change in apparent exponent at $k^* = 7$ separates the bulk multi-community population from a numerically thin upper tail. We name this tail the *carrier layer* – the $k \geq 7$ canonical humans (nine individuals after bot/phantom filtering, red triangles in Figure 3C–D, panel-C tail) – and adopt this term throughout the rest of the paper to refer to the contributor population that the analyses below and in Sections 4.4–4.5 show to repeatedly cross community boundaries and absorb cross-community integration cost on behalf

of the rest of the ecosystem. Among multi-community contributors, the home community (the modal community by commit count) typically still dominates: most points in Figure 3D fall below the diagonal, with a median share of inter-community commits equal to 25% (mean 27%). Restricted to the carrier layer, inter-community commits scale sublinearly with intra-community commits, $n_{\text{inter}} \sim n_{\text{intra}}^{0.53(9)}$ ($R^2 = 0.82$, $p < 10^{-3}$), whereas the per-bin median across all 966 multi-community contributors is essentially flat in n_{intra} [slope 0.06(5), $p = 0.26$, $R^2 = 0.15$]: the carrier layer therefore sits roughly a decade above the typical contributor at any given n_{intra} and absorbs the inter-community workload disproportionately. The boundary-crossing minority therefore remains anchored in a home community while distributing a substantial part of its activity elsewhere – a pattern whose collaboration-depth consequences are unpacked in Section 4.5.

A complementary, predictive angle on the importance of community links comes from a repository-level forecasting exercise reported in Supplementary S.6. Two random-forest regressions of six-month commit volume per repository are compared: one with the previous six months of activity as a feature (capturing auto-regressive memory), and one without. Removing the temporal-memory term reveals that structural features – the number of community links, the inter-/intra-community pull-request ratio, repository-level link-density summaries, and lifetime – retain substantial explanatory power. This is consistent with the cross-community contributor story above: ecosystem embedding is observable enough at the repository scale to forecast future activity even when short-run persistence is removed, providing an additional, independent line of evidence that cross-community structure carries predictive weight beyond local dynamics.

4.4 Community survival and the cohort hazard

The cross-community contributor layer identified above sustains boundary work, but it does not by itself sustain communities. To characterise community survival we compute, for each non-singleton community, the time from birth to its first year below 5% of its mean yearly commit activity that is never recovered (Methods Section 3; full procedure and threshold sensitivity in Supplementary S.7.1). Of the 163 non-singleton communities, 55 have entered residual by 2021 and 108 are right-censored at the observation horizon $Y_{\text{end}} = 2021$. Figure 4A plots the per-community time-to-residual against birth year, with markers coloured by mean yearly commits and red edges marking censored cases. Communities born in 2001–2010 sit close to the censoring envelope (most have not yet entered residual after 11–20 years); the 2015–2018 cohorts are sharply bimodal between very short non-residual spans and a tail of censored cases.

The cohort effect is not an artefact of shorter observation windows. Following the standard right-censored survival framework [61, 62], Figure 4A' reports the per-cohort annual hazard,

$$h(\text{cohort}) = \frac{\#\{\text{events in cohort}\}}{\sum_{c \in \text{cohort}} (y_c^* - b_c + 1)}, \quad (3)$$

which normalises by years-at-risk and is therefore not mechanically driven by the geometric censoring envelope $Y_{\text{end}} - b_c + 1$. Pre-2010 cohorts sit at 0–0.05 yr⁻¹; the hazard

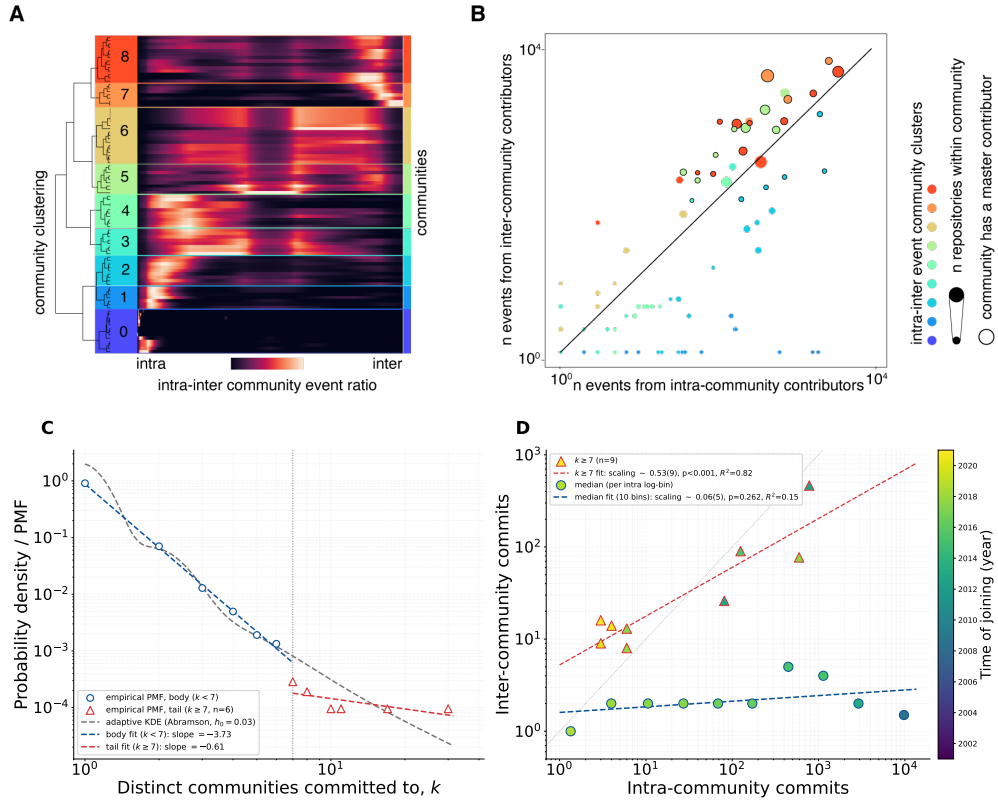


Fig. 3 Cross-community collaboration at the community and contributor scales. **A.** Heatmap and dendrogram clustering the 163 non-singleton communities (rows) by their intra-/inter-community pull-request event ratio (gradient fill); cluster colours and IDs shown in the dendrogram. **B.** Communities ordered by within-community (x) and across-community (y) event counts; dot colour follows the panel-A clustering, size encodes constituent repositories, contoured dots flag communities with active cross-community contributors. **C.** Empirical PMF of contributor breadth k on 10,490 canonical humans after bot/phantom filtering (Methods Section 3.1): blue open circles for the body ($k < 7$) and red open triangles for the tail ($k \geq 7$, $n = 9$). Adaptive Abramson KDE on $\log_{10} k$ in grey dashed. OLS body and tail power-law fits in matching colours (blue/red dashed) with breakpoint $k^* = 7$ chosen by minimum body+tail SSR (slopes and SSR scan in main text and Supplementary S.5.1). **D.** Per-contributor intra- vs. inter-community commit split, with markers and colours matching the panel-C regimes. Red triangles ($n = 9$): humans at $k \geq 7$ (panel-C tail). Blue circles: per-bin medians across ten log-spaced n_{intra} bins over the 966 multi-community contributors (panel-C body in aggregate). Marker fill: year of first intra-community commit (viridis over 2001–2021, matching Figure 2B). Dashed lines: OLS power-law fits in matching regime colours (exponents in main text); dotted diagonal: $n_{\text{inter}} = n_{\text{intra}}$.

rises sharply for the 2015–2018 cohorts and peaks at 0.193 yr^{-1} for the 2018 cohort ($n = 25$). Communities born after the community-count peak transition (~ 2017) are intrinsically more likely to drop into residual within any given year, consistent with the broader observation that abandonment and reduced maintenance are themselves cohort-structured features of the OSS landscape [9, 63].

The cross-community contributor layer is associated with longer survival at the community scale. Figure 4B shows Kaplan–Meier non-residual probability stratified by tertiles of inter-community pull-request share: the high-share tertile sustains a ~ 0.55

ten-year non-residual probability against ~ 0.30 for the low-share tertile, with a multi-group log-rank statistic of $\chi^2 = 21.9$ ($p = 1.8 \times 10^{-5}$). A multivariate Cox proportional-hazards model controlling for cohort and size confirms the protective association of the inter-community pull-request share. We report each predictor’s effect as a *hazard ratio* ($HR = \exp(\beta)$, the multiplicative change in the per-year residualisation hazard for a one-unit increase in the predictor: $HR < 1$ is protective, $HR > 1$ accelerates the event), accompanied by its 95% Wald *confidence interval* (CI, the 2.5%–97.5% range of the hazard ratio under the asymptotic normality of the maximum-likelihood estimate). For the inter-community pull-request share we obtain $HR = 0.11$, 95% CI [0.02, 0.61], $p = 0.012$, with model concordance $C = 0.84$; the full model is reported in Table 1 and discussed in Supplementary S.7.2.

Panel C of Figure 4 stratifies the same survival outcome by tertiles of the symmetric inter-community degree $\log_{10}(1 + d_c^{ext})$ – the count of *distinct* other communities a focal community exchanges commits with, irrespective of pull-request volume. The univariate separation is sharper still than in panel B: the high-degree tertile sustains a ~ 0.95 ten-year non-residual probability against ~ 0.10 in the lowest tertile (multi-group log-rank $\chi^2 = 49.1$, $p = 2.2 \times 10^{-11}$). In the multivariate Cox model, however, this effect attenuates substantially ($HR = 0.19$, 95% CI [0.02, 2.09], $p = 0.176$): much of the apparent univariate protection from external reach is mediated by community size, which is itself protective and strongly correlated with the number of external communities a community manages to engage. The cross-community degree therefore reads as a partial proxy for community resourcedness rather than as an independent causal mechanism, but the qualitative ordering – communities with broader cross-community reach are dramatically more likely to remain non-residual – is unambiguous in the data, and is consistent with the carrier-layer reading: communities that succeed in being engaged by carrier-layer contributors are also the ones that survive longest. We read this as an end-of-window association rather than a causal-direction test: communities that survived longer accumulated more cross-community pull-requests in part because they were around to receive them. The recognition mechanism documented at the contributor scale (Section 4.5, Supplementary S.8.1) describes how cross-community work is sustained *once it occurs* – by the carrier layer introduced in Section 4.3, whose repeat cross-boundary submissions absorb integration friction at near-intra-community cost. The cohort hazard documents that survival depends on more than the existence of this layer: late-cohort communities are over-represented among the residualisation events even though the carrier layer itself is stable on aggregate. The carrier layer therefore makes cross-boundary work cheap when present, but cannot, by itself, equalise cohort-level access to that work; the carrier-layer-and-cohort tension is the substrate of the broader optimisation/resilience discussion we return to in Section 5.

4.5 Boundary Friction and Collaboration Depth

Cross-community coupling metrics reported above capture the *breadth* of inter-community collaboration – how much of it takes place and where. A complementary question, motivated in Background Section 2, concerns its *depth*: how contested, sustained, and costly cross-community work is in practice. The primary commit+PR

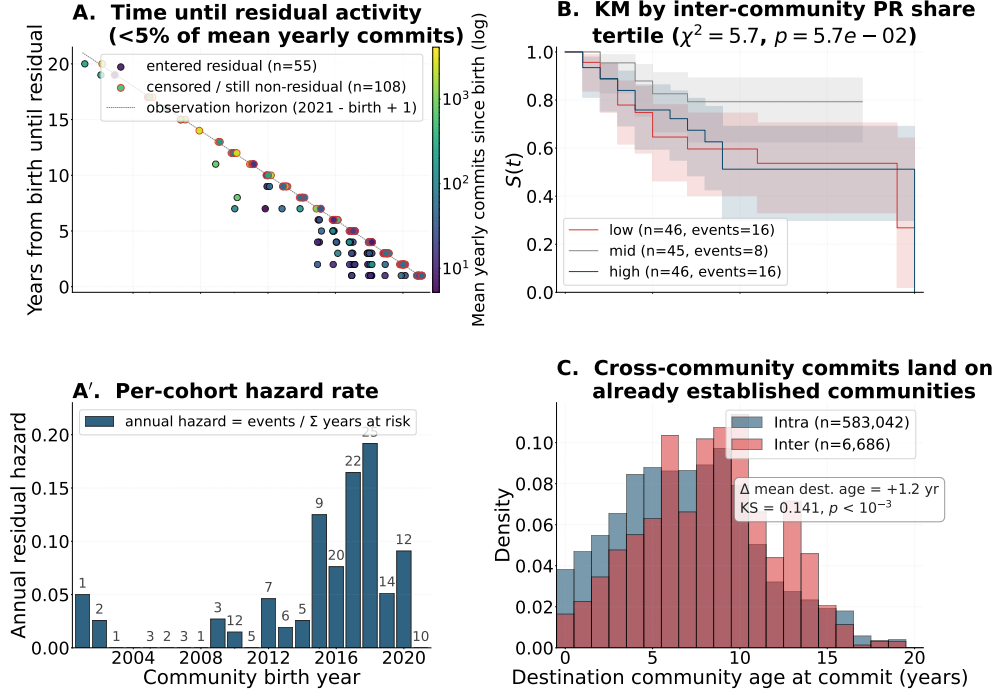


Fig. 4 Community survival, per-cohort hazard, and Kaplan–Meier stratifications by cross-community connectivity. Definitions for the residual phase, the per-cohort hazard, and d_c^{ext} are given in Methods Section 3.4. Panels A and A' share the birth-year x -axis on the left; panels B and C share the years-from-birth x -axis on the right. **A.** Per-community time from birth to residual (55 events, 108 right-censored at $Y_{\text{end}} = 2021$); marker fill is mean yearly commits since birth, red edges flag censored communities, dashed line is the geometric censoring envelope. **A'.** Per-cohort annual hazard rate of entering residual; bar labels are cohort sizes. The hazard rises an order of magnitude between pre-2010 cohorts and the 2015–2018 cohorts (peaking at 0.193 for the 2018 cohort). **B.** Kaplan–Meier non-residual probability by tertiles of inter-community pull-request share (multi-group log-rank $\chi^2 = 21.9, p = 1.8 \times 10^{-5}$). **C.** Kaplan–Meier non-residual probability by tertiles of $\log_{10}(1 + d_c^{\text{ext}})$, the symmetric inter-community degree ($\chi^2 = 49.1, p = 2.2 \times 10^{-11}$). The accompanying multivariate Cox proportional-hazards model is in Table 1.

dataset preserves only merged pull requests; to probe depth directly we draw on the second GitHub Archive event stream described in Methods Section 3.1 and derive five depth indicators – pull-request acceptance rate, integration latency, review-state mix, issue discussion depth, and contributor retention after a boundary crossing. Each indicator is computed both globally and stratified by whether the submitter’s home community matches the recipient repository’s community, yielding a principled intra-versus inter-community comparison that is summarised in Figure 5.

At the *pull-request* level, boundary-crossing contributions are markedly more costly on every depth indicator (Figure 5). Of the 83,075 closed pull requests for which the submitter’s home community can be identified, intra-community submissions are accepted at 81.9% whereas inter-community submissions are accepted at 61.1%, a 20.8 percentage-point gap that is highly significant ($\chi^2 = 113.9, p < 10^{-3}$; panel A). Integration latency amplifies the same pattern: the median time between a pull request’s creation and its terminal state is 19.2 hours within-community versus 38.3

Table 1 Multivariate Cox proportional-hazards model for community residualisation on $n = 163$ non-singleton Louvain communities (55 events, 108 censored at $Y_{\text{end}} = 2021$; concordance $C = 0.843$). Hazard ratios with 95% Wald confidence intervals; the cross-communities connectivity covariates are tested while controlling for cohort and size. **Bold rows** mark predictors significant at $p < 0.05$.

predictor	HR	95% CI lower	95% CI upper	p
Birth year	1.18	1.03	1.35	0.021
\log_{10} # repositories	0.21	0.01	3.87	0.292
\log_{10} # contributors	0.39	0.15	1.02	0.055
Inter-community PR share	0.11	0.02	0.61	0.012
\log_{10} # external communities reached	0.19	0.02	2.09	0.176
Share of contributors with $k \geq 2$	4.72	0.39	56.6	0.221

hours across-community for merged PRs (ratio 2.0), and widens to 40.6 hours versus 168.0 hours for rejected PRs (ratio 4.1; $p < 10^{-3}$; panel B). A smaller secondary signal echoes the same pattern: among the merged pull-requests with at least one review event (post-2017 coverage 27%), 13.0% of intra-community PRs receive at least one `CHANGES_REQUESTED` review against 8.3% for inter-community PRs (Fisher odds ratio 1.66, $p = 0.008$), so inter-community contributions are not merely slower but are handled more *binarily*, with less iterative revision and a higher share of outright rejection [31]. At the *issue* level, the same boundary accrues coordination cost in deliberation rather than code review: across 164,125 issues, inter-community issues attract a median of 2 comments against 1 for intra-community issues (means 4.08 versus 2.84; Mann–Whitney $p < 10^{-3}$; panel C), paralleling Kittur et al.’s observation that cross-boundary work in peer-produced systems is reflected in talk-page volume [29].

The cross-community work that bridges these costs is concentrated in a very thin layer of contributors – the same minority isolated at the contributor scale in Figure 3C–D. Of the 10,490 canonical human contributors after bot/phantom filtering (Methods Section 3.1), 883 (8.4%) ever author a merged pull request that crosses a community boundary; the top 10 produce 37% of all 4,015 inter-community merged pull requests, the top 50 produce 54%, and the top 250 produce 80%. Without the filter, `dependabot[bot]` alone would account for $\sim 24\%$ of the unfiltered 5,612 inter-community pull-request volume. Commit-level breadth and pull-request-level cross-boundary activity are nearly identically rank-ordered across canonical humans (Spearman $\rho = 0.96$): the same minority that commits to multiple communities produces essentially the entire inter-community pull-request volume. Within the 255 contributor–repository pairs with three or more cross-community merged pull requests, a fixed-effects regression of log-turnaround on within-pair sequence index yields a small but significant negative slope ($\beta = -0.0010$, $p = 0.005$); we report this only as a within-pair effect, since the marginal medians by sequence index in fact *rise* with sequence due to selection (pairs that recur tend to involve repositories with longer baseline turnaround).

This carrier layer is also unevenly distributed across the ecosystem and visibly fragile. Of the 163 non-singleton communities, 64 (39%) have never had a single human

contributor with cross-community pull-request experience; in another 21 communities (13%) cross-community contributors are present in the historical record but *all* have gone dormant in the final twelve months of the observation window (no commit since 2021-05-31). Together, 85 communities (52%) currently lack any active cross-community contributor at all, and only 78 (48%) retain at least one. The depth indicators in Figure 5 therefore portray a coherent pattern we call *friction with stable trust*: cross-community work is measurably more contested on every dimension, yet is sustained by a thin, identifiable layer of contributors whose presence in a community is structurally consequential rather than incidental. Modular ecosystems are workable not because friction is absent, but because a small set of recurring contributors absorbs it; the nearly half of communities that currently lack any active cross-community contributor are correspondingly more exposed to fragmentation when boundary-crossing collaboration is needed.

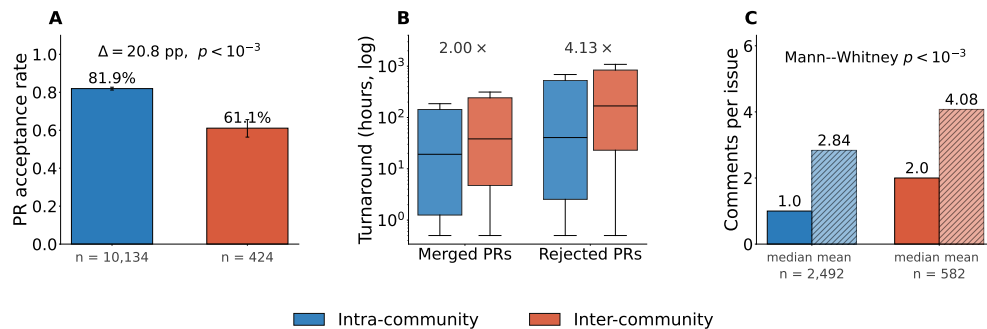


Fig. 5 Boundary friction at the pull-request and issue level. Each panel compares an intra-community to an inter-community slice of the same depth indicator (colour legend below); error bars are Wilson 95% confidence intervals on proportions and per-bar sample sizes are annotated. **A.** Pull-request acceptance rate, per (repository, PR number) pair on the terminal state; the gap is 20.8 pp. **B.** Turnaround distribution split by outcome (merged vs. rejected); box heights show the IQR around the median; \times -labels are the inter-to-intra median ratio. **C.** Median (solid) and mean (hatched) comments per issue, by the issue author’s home community relative to the recipient repository. The smaller secondary CHANGES_REQUESTED signal is reported in the main text and stratified by author breadth k in Supplementary S.8.1.

5 Discussion

Our analyses jointly support a *recognition / repeat-relationship account* of sustained cross-boundary work in modular socio-technical ecosystems. Boundary-crossing pull-requests are accepted 20.8 percentage points less often than within-community ones (61.1% vs. 81.9%), take two to four times longer to integrate, and attract a more binary review pattern – gaps that sit in the range the peer-production literature associates with active coordination effort at group boundaries rather than technical noise [29–32]. Stratifying these depth indicators by the contributor’s commit-level breadth k shows that the friction is not a permanent property of the boundary: inter-community PR acceptance climbs from 42% at $k=1$ to 87% at $k=5-9$, and turnaround compresses

three-fold from 147h to 49h. The cross-community contributor layer at $k \geq 5$ submits inter-community pull-requests at near-intra-community speed and acceptance; the residual friction is concentrated in low- k one-off submitters whose cross-community contribution is a single contested PR. The mechanism is one of recognition: contributors with established cross-boundary presence have already accumulated the trust that low- k contributors must build during a single contested submission.

This carrier of inter-community collaboration is numerically thin. Of 10,490 canonical human contributors after bot and phantom-identity filtering, only 883 (8.4%) ever author a merged pull-request that crosses a community boundary; within that subset the top 10 produce 37% of all 4,015 inter-community merged pull-requests, the top 50 produce 54%, and the top 250 produce 80%. The same minority appears at the commit level: 91% of contributors commit to a single community, and the small subset that commits to multiple communities is nearly identically rank-ordered with the cross-boundary pull-request authors (Spearman $\rho = 0.96$). The carrier layer is also unevenly distributed across the ecosystem: 64 of the 163 non-singleton communities (39%) never host a human contributor with cross-community pull-request experience, and a further 21 (13%) had one or more historically but have lost them to twelve-month dormancy by the end of the observation window. Together, 52% of communities currently lack any active cross-community contributor. Read against Benkler’s account of commons-based peer production [8], this pattern suggests that the health of an OSS ecosystem’s inter-community links does not rest on friction being absent but on whether a small subset of contributors actively spans community boundaries, mirroring the keystone roles identified in earlier OSS literature [44, 45, 51]. The static-Cox analysis in Supplementary S.7.2 establishes this as an end-of-window association, not as a causal-direction test: the recognition mechanism documented here describes how cross-boundary work is sustained *once it occurs*, and the 52% figure is a fragility signal at the carrier of inter-community collaboration rather than a demonstrated structural risk to community survival. The same reading extends to the second cross-community survival signal (Figure 4C): the symmetric inter-community degree d_c^{ext} separates ten-year non-residual probabilities of ~ 0.95 for the highest tertile from ~ 0.10 for the lowest (log-rank $\chi^2 = 49.1$, $p = 2.2 \times 10^{-11}$), but the multivariate Cox attenuates the effect substantially because external reach is mediated by community size. The cross-community degree therefore reads, like the inter-community PR share, as a partial proxy for community resourcedness rather than as an independent causal mechanism for survival; what both panels agree on is the qualitative ordering – communities that succeed in being engaged across many boundaries are dramatically more likely to remain non-residual, the same population on which the carrier layer’s repeat cross-boundary submissions land.

What we can and cannot optimise for.

The observation window closes at May 2022, immediately before the mainstream diffusion of large-language-model (LLM) assisted development tools [64, 65]. The depth indicators reported here therefore characterise *human-coordinated* boundary-crossing in OSS at ecosystem scale, before this technology became part of the day-to-day workflow. Each indicator has a plausible mechanism by which AI-assisted authoring and

review could shift it: acceptance might rise if assistants raise baseline code quality or fall if they enable lower-effort contributions; latency might compress as AI summarisation triages faster; the review-state mix might tilt toward iterative revision as suggestions become cheap to apply; and the recognition mechanism itself might attenuate if AI lowers the per-contribution cost of crossing community boundaries. We therefore present the corpus and the depth-indicator panel as a measurable *pre-AI baseline*: replicating the same panel on a 2023–2026 OSS corpus would let claims about “the impact of AI on open collaboration” rest on side-by-side ecosystem-scale evidence rather than on rhetoric. Three AI-driven shifts deserve specific attention in such a follow-up. First, on *trust-building*: the friction stratification of Section 4.5 attributes the inter-community pull-request acceptance gap to a recognition cost that low- k submitters pay during a single contested submission, and AI-mediated review and contextual summarisation could in principle compress that cost by surfacing the contribution’s provenance and prior code in a form that a busy maintainer can absorb cheaply, attenuating the gap between one-off and repeat cross-boundary submitters; whether this happens in practice depends on whether AI suggestions are read as a credible trust signal or as another low-effort artefact, an open question on which the existing usability and security evidence is mixed [66, 67]. Second, on *cohort-level access to cross-community attention*: late-cohort communities in our corpus are sharply over-represented among residualisation events (Section 4.4) and the 52% of communities currently without an active cross-community contributor are not concentrated in any single cohort, so the carrier-layer supply we document does not, on its own, reach late-born communities at the rate the recognition mechanism would require – though we do not directly test the contributor-side routing that would explain the gap. Cognitive substrates that could plausibly underlie an asymmetric routing of contributor attention toward already-visible destinations include the *availability heuristic* of Tversky and Kahneman [68] and a *status-quo bias* [69]; AI-driven recommenders trained on activity traces of the kind we report here would, if blindly applied, be well placed to amplify any such asymmetry [70, 71], and counteracting it would require explicitly fairness-aware routing of contributor attention towards under-engaged communities – a measurable design objective rather than a hope. Third, on *alleviating the cohort hazard*: the survival-side counterpart to the under-served-late-cohort pattern is the per-cohort residualisation hazard documented in Section 4.4, which rises an order of magnitude between pre-2010 cohorts and the 2018 cohort. AI tools that lower the operational entry cost for small or late-cohort communities – automated dependency-update pull-requests, AI-assisted documentation, generative authoring of boilerplate code – could in principle reduce that hazard by substituting for some of the maintenance labour the carrier layer is currently asked to provide [64, 65]. There are limits, however, to what such an optimisation can deliver. The mechanisms our analyses surface – recognition (Section 4.5) and the cohort-structured fragility of the carrier layer (Section 4.4) – are not failure modes that an efficiency-oriented optimiser can simply remove, because the same dynamics that produce the friction also produce the trust on which the carrier layer’s near-intra-community acceptance rests; the Highly Optimised Tolerance literature warns explicitly that systems optimised for expected workloads become acutely fragile to unanticipated shocks [35, 40, 72] – how that fragility would

unfold in an AI-mediated OSS ecosystem, and what governance or platform mechanisms could pre-empt it, remains an open question at this stage of the technology’s diffusion. AI-assisted productivity gains in OSS ecosystems are therefore best read as a question of what *can* be optimised away (boilerplate, dependency hygiene, documentation drift) versus what *should not* be (the human social fabric of trust accumulation that the recognition mechanism rests on, and the bot/human identification boundary on which our identity reconciliation depends – given the thinness of the carrier layer, nine humans at $k \geq 7$, even small misclassifications between human and AI agents would qualitatively shift the picture). The depth-indicator panel of this paper provides the measurement substrate to tell those two apart. A deeper question, however, hangs over the next decade of OSS production. The technology is moving fast enough that an increasing share of code on public platforms is now authored or co-authored by large language models [64, 65, 73], and it is genuinely uncertain how much of the contributor distribution itself will remain human in any meaningful sense by the end of this decade. The carrier layer the present paper isolates – a thin tail of repeat cross-boundary humans on whom the cross-community fabric of a 464-repository ecosystem currently rests – is precisely the kind of human-mediated structure that an aggressive AI-substitution strategy could displace: directly, by routing cross-community pull-requests through LLM agents instead of repeat human contributors; and indirectly, by eroding the trust-accumulation mechanism on which the recognition gradient of Section 4.5 rests once authorship signals stop reliably indexing a human history of repeated cross-boundary engagement. Whether such a substitution is welfare-improving, and on what terms, is not a question optimisation alone can answer. *What we ultimately cannot optimise for is our own place in the digital societies these ecosystems prefigure*: the carrier layer is not just a piece of infrastructure to be made more efficient, it is part of how a community of humans recognises its own collective work, and that recognition is what an OSS-style commons ultimately rests on [8].

Digital societies and the scope of transfer.

Cybersecurity OSS is part of the digital infrastructure on which many societal functions rely, and OSS-like codes and processes already structure other domains of digital production: in live coding for music and performance, creators modify executable code in real time, often projecting it publicly and iterating through rapid, auditable edits that can be shared, remixed, and reused across a community [12, 13]; on Wikipedia, distributed editors recursively co-produce article quality through bipartite contributor–article cooperation patterns whose dynamics resemble those of OSS [14, 15]. In parallel, the broader epistemic environment in which open collaboration takes place is being reshaped by dramatic AI-driven advances in science – from near-experimental-accuracy protein structure prediction [16] and scaled materials discovery [74] to a generalised reframing of scientific discovery itself [17], with code-generation systems now matching competitive-programming performance [73] – which makes trustworthy validation, provenance, and review at the boundaries of communities the binding constraint, not authoring throughput. A plausible vision – not tested here as a welfare claim – is that robust digital societies will need institutions and infrastructures that preserve community-level autonomy *and* workable cross-boundary coordination

under uncertainty; OSS ecosystems are historically where those tensions first became observable at scale through public traces. This systems perspective has broader implications: as digital infrastructures increasingly shape the design, coordination, and adaptation of physical systems – urban mobility [18], energy grids [19], and civic platforms [20, 75] – the architecture of open, adaptive software ecosystems becomes directly relevant to the governance of digital societies [4, 5, 76]. The recognition mechanism documented here is, in principle, transferable to any time-evolving bipartite interaction system in which boundary-crossing carries an integration cost – citizen-science platforms, federated open-data ecosystems, multi-team enterprise software – and the measurement strategy we deploy (carrier-layer identification, friction-gradient stratification, and survival analysis, Sections 4.3–4.5) carries over directly whenever an analogous interaction graph can be reconstructed. We treat parallels to urban, mobility, or energy systems as hypothesis-generating, not as findings of this paper.

Limitations.

Our sample is the Rawsec Cybersecurity Inventory as of May 2022; productive interactions extend beyond it. The $k \geq 7$ cross-community contributor threshold used throughout the Results is data-driven (Supplementary S.5.1) rather than ad hoc, but it is still a single thresholded summary of an affiliation distribution that is otherwise continuous. The static-Cox analysis (Supplementary S.7.2) is an end-of-window association; we did not in this submission re-fit it with time-varying connectivity covariates, which would be the proper test of causal protection by the carrier layer and which we identify as the principal direction for follow-up work. Sentiment-level review-comment analysis, organisational-affiliation proxies for institutional support, and off-platform coordination remain out of scope. Future work could combine ethnography or surveys with network traces, extend the inventory beyond cybersecurity, and examine how embedded coding assistants change collaboration patterns on platforms, including fairness and transparency risks [70, 71, 77].

6 Conclusion

This paper measures the architecture of cross-boundary collaboration in a longitudinal cybersecurity OSS corpus. At the ecosystem scale, per-community contributor count scales superlinearly with repository count ($n_{\text{contributors}} \sim n_{\text{repos}}^{1.4}$) and community formation follows a logistic trajectory whose carrying capacity is reached around 2018. Within that maturing structure we isolate a thin *carrier layer* – nine canonical humans at $k \geq 7$ – that absorbs cross-community integration cost at near-intra-community speed once present, but is unevenly distributed across the 163 non-singleton communities and cannot, by itself, equalise the cohort-level hazard of residualisation. Late-cohort communities are over-represented among the residualisation events even though the carrier-layer supply itself is stable on aggregate, leaving them under-served on cross-community attention. We do not equate GitHub collaboration graphs with cities or critical-infrastructure networks; what we offer is a measurement template – carrier-layer identification, friction-gradient stratification,

and survival analysis – transportable to any time-evolving bipartite interaction system in which boundary-crossing carries an integration cost.

Because the corpus closes just before the mainstream diffusion of large-language-model coding assistants, the friction gradient, the carrier-layer thinness, and the cohort hazard together constitute a measurable pre-AI baseline against which AI-mediated OSS ecosystems can be compared. What can be optimised away in OSS production – boilerplate, dependency hygiene, documentation drift – and what cannot – the human social fabric of trust accumulation on which the recognition mechanism rests – is the substantive question this baseline now lets the next decade of OSS scholarship ask in measurement terms rather than in rhetoric. The carrier layer is not just infrastructure to be made more efficient: it is part of how a community of humans recognises its own collective work, and that is what an OSS-style commons ultimately rests on.

Declarations

Data and Code Availability. The datasets generated and analyzed during the current study, as well as the code scripts used, are available in the repository <https://doi.org/10.17605/OSF.IO/5RWEK>.

Competing interests. Not applicable.

Funding. Thomas Maillart (T.M.), Lucia Gomez Tejeiro (L.G.T.) and Thibaut Chataing (T.C.) acknowledge financial support by armasuisse Science and Technology (S+T).

Author contributions. T.M. and L.G.T conceptualized the research. L.G.T, T.M. and T.C. performed the analyses, T.M., L.G.T wrote the manuscript. Julian Jang-Jaccard (J.J.J.) and Alain Mermoud (A.M.) revised and improved the manuscript.

Use of large language models (LLMs) and AI assistants. During the preparation of this work, the authors used large-language-model assistants (Claude and GitHub Copilot) to support code refactoring and figure-generation scripts, and to copy-edit prose for clarity. After using these tools, the authors reviewed and edited the output as needed and take full responsibility for the content of the publication. LLMs do not satisfy authorship criteria and are not listed as authors; all research questions, study design, analytical decisions, interpretation of results, and conclusions are the authors' own. This disclosure follows the Springer Nature editorial policy on the use of generative AI in scientific writing.

References

- [1] Lerner, J., Pathak, P.A., Tirole, J.: The Dynamics of Open-Source Contributors. *American Economic Review* **96**(2), 114–118 (2006) <https://doi.org/10.1257/000282806777211874> . Accessed 2021-03-31
- [2] Sharma, R., Dangi, S., Mishra, P.: A Comprehensive Review on Encryption based Open Source Cyber Security Tools. In: 2021 6th International Conference on Signal Processing, Computing and Control (ISPCC), pp. 614–619

- (2021). <https://doi.org/10.1109/ISPC53510.2021.9609369> . ISSN: 2643-8615.
<https://doi.org/10.1109/ISPC53510.2021.9609369>
- [3] Floridi, L.: *The Fourth Revolution: How the Infosphere Is Reshaping Human Reality*. Oxford University Press, Oxford (2014)
- [4] Helbing, D., Mahajan, S., Carpentras, D., Menendez, M., Pournaras, E., Thurner, S., Verma, T., Arcaute, E., Batty, M., Bettencourt, L.M.A.: Co-creating the future: participatory cities and digital governance. *Philosophical Transactions of the Royal Society A: Mathematical, Physical and Engineering Sciences* **382**(2285), 20240113 (2024) <https://doi.org/10.1098/rsta.2024.0113>
- [5] Wang, H., Peng, G., Du, H.: Digital economy development boosts urban resilience—evidence from China. *Scientific Reports* **14**, 2925 (2024) <https://doi.org/10.1038/s41598-024-52191-4> . Accessed 2025-09-17
- [6] Benkler, Y.: Coase’s Penguin, or, Linux and ”The Nature of the Firm”. *The Yale Law Journal* **112**(3), 369 (2002) <https://doi.org/10.2307/1562247>
- [7] Lerner, J., Tirole, J.: The Scope of Open Source Licensing. *Journal of Law, Economics, and Organization* **21**(1), 20–56 (2005) <https://doi.org/10.1093/jleo/ewi002>
- [8] Benkler, Y.: *The Penguin and the Leviathan: How Cooperation Triumphs over Self-Interest*, 1st edn. Crown Business, ??? (2011). Published: Hardcover. <https://www.worldcat.org/isbn/0385525761>
- [9] Coelho, J., Valente, M.T., Silva, L.L., Shihab, E.: Identifying unmaintained projects in github. In: *Proceedings of the 12th ACM/IEEE International Symposium on Empirical Software Engineering And Measurement. ESEM ’18*, pp. 1–10. Association for Computing Machinery, New York, NY, USA (2018). <https://doi.org/10.1145/3239235.3240501> . <https://doi.org/10.1145/3239235.3240501> Accessed 2022-11-08
- [10] Paschali, M.-E., Ampatzoglou, A., Bibi, S., Chatzigeorgiou, A., Stamelos, I.: Reusability of open source software across domains: A case study. *Journal of Systems and Software* **134**, 211–227 (2017) <https://doi.org/10.1016/j.jss.2017.09.009> . Accessed 2025-09-17
- [11] Ladisa, P., Plate, H., Martinez, M., Barais, O.: Taxonomy of Attacks on Open-Source Software Supply Chains. arXiv. arXiv:2204.04008 [cs] (2022). <https://doi.org/10.48550/arXiv.2204.04008> . <https://doi.org/10.48550/arXiv.2204.04008> Accessed 2023-03-27
- [12] Collins, N., McLean, A., Rohrhuber, J., Ward, A.: Live coding in laptop performance. *Organised Sound* **8**(3), 321–330 (2003) <https://doi.org/10.1017/S135577180300030X>

- [13] Collins, N.: Live Coding of Consequence. *Leonardo* **44**(3), 207–211 (2011) https://doi.org/10.1162/LEON_a_00164
- [14] Wilkinson, D.M., Huberman, B.A.: Cooperation and quality in wikipedia. In: Proceedings of the 2007 International Symposium on Wikis. WikiSym '07, pp. 157–164. Association for Computing Machinery, New York, NY, USA (2007). <https://doi.org/10.1145/1296951.1296968> . <https://doi.org/10.1145/1296951.1296968> Accessed 2022-11-08
- [15] Klein, M., Maillart, T., Chuang, J.: The Virtuous Circle of Wikipedia: Recursive Measures of Collaboration Structures. In: Proceedings of the 18th ACM Conference on Computer Supported Cooperative Work & Social Computing. CSCW '15, pp. 1106–1115. Association for Computing Machinery, New York, NY, USA (2015). <https://doi.org/10.1145/2675133.2675286> . <https://doi.org/10.1145/2675133.2675286>
- [16] Jumper, J., Evans, R., Pritzel, A., Green, T., Figurnov, M., Ronneberger, O., Tunyasuvunakool, K., Bates, R., Žídek, A., Potapenko, A., Bridgland, A., Meyer, C., Kohl, S.A.A., Ballard, A.J., Cowie, A., Romera-Paredes, B., Nikolov, S., Jain, R., Adler, J., Back, T., Petersen, S., Reiman, D., Clancy, E., Zielinski, M., Steinegger, M., Pacholska, M., Berghammer, T., Bodenstein, S., Silver, D., Vinyals, O., Senior, A.W., Kavukcuoglu, K., Kohli, P., Hassabis, D.: Highly accurate protein structure prediction with AlphaFold. *Nature* **596**(7873), 583–589 (2021) <https://doi.org/10.1038/s41586-021-03819-2>
- [17] Wang, H., Fu, T., Du, Y., Gao, W., Huang, K., Liu, Z., Chandak, P., Liu, S., Van Katwyk, P., Deac, A., Anandkumar, A., Bergen, K., Gomes, C.P., Ho, S., Kohli, P., Lasenby, J., Leskovec, J., Liu, T.-Y., Manrai, A., Marks, D., Ramsundar, B., Song, L., Sun, J., Tang, J., Veličković, P., Welling, M., Zhang, L., Coley, C.W., Bengio, Y., Zitnik, M.: Scientific discovery in the age of artificial intelligence. *Nature* **620**(7972), 47–60 (2023) <https://doi.org/10.1038/s41586-023-06221-2>
- [18] Batty, M.: Big data, smart cities and city planning. *Dialogues in Human Geography* **3**(3), 274–279 (2013) <https://doi.org/10.1177/2043820613513390>
- [19] Farhangi, H.: The path of the smart grid. *IEEE Power and Energy Magazine* **8**(1), 18–28 (2010) <https://doi.org/10.1109/MPE.2009.934876>
- [20] Linders, D.: From e-government to we-government: Defining a typology for citizen coproduction in the age of social media. *Government Information Quarterly* **29**(4), 446–454 (2012) <https://doi.org/10.1016/j.giq.2012.06.003>
- [21] Maillart, T., Zhao, M., Grossklags, J., Chuang, J.: Given enough eyeballs, all bugs are shallow? Revisiting Eric Raymond with bug bounty programs. *Journal of Cybersecurity* **3**(2), 81–90 (2017) <https://doi.org/10.1093/cybsec/tyx008> . Accessed 2022-08-25

- [22] Gillard, S., Percia David, D., Mermoud, A., Maillart, T.: Efficient collective action for tackling time-critical cybersecurity threats. *Journal of Cybersecurity* **9**(1), 021 (2023) <https://doi.org/10.1093/cybsec/tyad021> . Accessed 2024-05-29
- [23] Wagner, C., Dulaunoy, A., Wagener, G., Iklody, A.: MISP: The Design and Implementation of a Collaborative Threat Intelligence Sharing Platform. In: *Proceedings of the 2016 ACM Workshop on Information Sharing and Collaborative Security (WISCS)*, pp. 49–56 (2016). <https://doi.org/10.1145/2994539.2994542> . <https://doi.org/10.1145/2994539.2994542>
- [24] Mockus, A., Fielding, R.T., Herbsleb, J.D.: Two Case Studies of Open Source Software Development: Apache and Mozilla. *ACM Transactions on Software Engineering and Methodology* **11**(3), 309–346 (2002)
- [25] Lee, G.K., Cole, R.E.: From a Firm-Based to a Community-Based Model of Knowledge Creation: The Case of the Linux Kernel Development. *Organization Science* **14**(6), 633–649 (2003)
- [26] Dabbish, L., Stuart, C., Tsay, J., Herbsleb, J.: Social coding in GitHub: transparency and collaboration in an open software repository. In: *Proceedings of the ACM 2012 Conference on Computer Supported Cooperative Work. CSCW '12*, pp. 1277–1286. Association for Computing Machinery, New York, NY, USA (2012). <https://doi.org/10.1145/2145204.2145396> . <https://doi.org/10.1145/2145204.2145396> Accessed 2022-11-08
- [27] Sornette, D., Maillart, T., Ghezzi, G.: How Much Is the Whole Really More than the Sum of Its Parts? $1 \boxplus 1 = 2.5$: Superlinear Productivity in Collective Group Actions. *PLoS ONE* **9**(8), 103023 (2014) <https://doi.org/10.1371/journal.pone.0103023>
- [28] Maillart, T., Sornette, D., Spaeth, S., Krogh, G.: Empirical Tests of Zipf’s Law Mechanism in Open Source Linux Distribution. *Physical Review Letters* **101**(21), 218701 (2008) <https://doi.org/10.1103/PhysRevLett.101.218701>
- [29] Kittur, A., Suh, B., Pendleton, B.A., Chi, E.H.: He says, she says: Conflict and coordination in Wikipedia. In: *Proceedings of the SIGCHI Conference on Human Factors in Computing Systems (CHI 2007)*, pp. 453–462. ACM, ??? (2007). <https://doi.org/10.1145/1240624.1240698> . <https://doi.org/10.1145/1240624.1240698>
- [30] Yasseri, T., Sumi, R., Rung, A., Kornai, A., Kertész, J.: Dynamics of conflicts in Wikipedia. *PLOS ONE* **7**(6), 38869 (2012) <https://doi.org/10.1371/journal.pone.0038869>
- [31] Tsay, J., Dabbish, L., Herbsleb, J.: Influence of social and technical factors for evaluating contribution in GitHub. In: *Proceedings of the 36th International Conference on Software Engineering (ICSE 2014)*, pp. 356–366. ACM, ??? (2014). <https://doi.org/10.1145/2568225.2568315> .

<https://doi.org/10.1145/2568225.2568315>

- [32] Halfaker, A., Kittur, A., Riedl, J.: Don't bite the newbies: how reverts affect the quantity and quality of Wikipedia work. In: Proceedings of the 7th International Symposium on Wikis and Open Collaboration (WikiSym 2011), pp. 163–172. ACM, ??? (2011). <https://doi.org/10.1145/2038558.2038585> . <https://doi.org/10.1145/2038558.2038585>
- [33] Holland, J.H.: Complex adaptive systems. *Daedalus* **121**(1), 17–30 (1992)
- [34] Mitchell, M.: *Complexity: A Guided Tour*. Oxford University Press, Oxford (2009)
- [35] Holling, C.S.: Resilience and Stability of Ecological Systems. *Annual Review of Ecology and Systematics* **4**, 1–23 (1973) <https://doi.org/10.1146/annurev.es.04.110173.000245>
- [36] Simon, H.A.: The Architecture of Complexity. *Proceedings of the American Philosophical Society* **106**(6), 467–482 (1962). Publisher: American Philosophical Society. Accessed 2025-07-16
- [37] Merton, R.K.: The Matthew Effect in Science: The reward and communication systems of science are considered. *Science* **159**(3810), 56–63 (1968) <https://doi.org/10.1126/science.159.3810.56>
- [38] Barabási, A.-L., Albert, R.: Emergence of Scaling in Random Networks. *Science* **286**(5439), 509–512 (1999) <https://doi.org/10.1126/science.286.5439.509>
- [39] Albert, R., Jeong, H., Barabási, A.-L.: Error and Attack Tolerance of Complex Networks. *Nature* **406**(6794), 378–382 (2000) <https://doi.org/10.1038/35019019>
- [40] Carlson, J.M., Doyle, J.: Highly Optimized Tolerance: Robustness and Design in Complex Systems. *Physical Review Letters* **84**(11), 2529–2532 (2000) <https://doi.org/10.1103/PhysRevLett.84.2529> . Publisher: American Physical Society. Accessed 2025-07-16
- [41] Stöger, F., Birge-Lee, H., Giuliani, G., Subira-Nieto, J., Perrig, A.: BGP Vortex: Update Message Floods Can Create Internet Instabilities, pp. 3613–3629 (2025). <https://www.usenix.org/conference/usenixsecurity25/presentation/stoeger> Accessed 2025-09-05
- [42] Bak, P., Tang, C., Wiesenfeld, K.: Self-organized Criticality: An Explanation of the 1/f Noise. *Physical Review Letters* **59**(4), 381–384 (1987) <https://doi.org/10.1103/PhysRevLett.59.381>
- [43] Saichev, A.I., Maillart, T., Sornette, D.: Hierarchy of temporal responses of multivariate self-excited epidemic processes. *The European Physical Journal B* **86**(4),

1–19 (2013) <https://doi.org/10.1140/epjb/e2013-30493-9>

- [44] Maillart, T., Sornette, D.: Aristotle vs. Ringelmann: On superlinear production in open source software. *Physica A: Statistical Mechanics and its Applications* **523**, 964–972 (2019) <https://doi.org/10.1016/j.physa.2019.04.130>
- [45] Scholtes, I., Mavrodiev, P., Schweitzer, F.: From Aristotle to Ringelmann: A Large-scale Analysis of Team Productivity and Coordination in Open Source Software Projects. *Gesellschaft für Informatik e.V., ???* (2016). Accepted: 2017-06-21T07:37:17Z ISSN: 1617-5468. <https://dl.gi.de/handle/20.500.12116/717> Accessed 2021-03-23
- [46] Murić, G., Abeliuk, A., Lerman, K., Ferrara, E.: Collaboration Drives Individual Productivity. *Proceedings of the ACM on Human-Computer Interaction* **3**(CSCW), 74–17424 (2019) <https://doi.org/10.1145/3359176> . Accessed 2021-03-23
- [47] Maillart, T., Gomez, L., Lombard, E., Nolte, A., Pisano, F.: Computational diplomacy: how ‘hackathons for good’ feed a participatory future for multilateralism in the digital age. *Philosophical Transactions of the Royal Society A: Mathematical, Physical and Engineering Sciences* **382**(2285) (2024) <https://doi.org/10.1098/rsta.2024.0103> . Publisher: The Royal Society. Accessed 2025-08-24
- [48] Fortunato, S.: Community detection in graphs. *Physics Reports* **486**(3), 75–174 (2010) <https://doi.org/10.1016/j.physrep.2009.11.002>
- [49] De Meo, P., Ferrara, E., Fiumara, G., Provetti, A.: Generalized Louvain method for community detection in large networks. In: 2011 11th International Conference on Intelligent Systems Design and Applications, pp. 88–93 (2011). <https://doi.org/10.1109/ISDA.2011.6121636> . ISSN: 2164-7151. <https://doi.org/10.1109/ISDA.2011.6121636>
- [50] Powell, W.W., White, D.R., Koput, K.W., Owen-Smith, J.: Network Dynamics and Field Evolution: The Growth of Interorganizational Collaboration in the Life Sciences. *American Journal of Sociology* **110**(4), 1132–1205 (2005) <https://doi.org/10.1086/421508>
- [51] Fleming, L., Mingo, S., Chen, D.: Collaborative Brokerage, Generative Creativity, and Creative Success. *Administrative Science Quarterly* **52**(3), 443–475 (2007)
- [52] Newman, M.E.J.: Scientific collaboration networks. II. Shortest paths, weighted networks, and centrality. *Physical Review E* **64**(1), 016132 (2001) <https://doi.org/10.1103/PhysRevE.64.016132>
- [53] Latapy, M., Magnien, C., Del Vecchio, N.: Basic notions for the analysis of large two-mode networks. *Social Networks* **30**(1), 31–48 (2008) <https://doi.org/10.1016/j.socnet.2007.04.006>

- [54] McInnes, L., Healy, J., Melville, J.: UMAP: Uniform Manifold Approximation and Projection for Dimension Reduction. arXiv. arXiv:1802.03426 [cs, stat] (2018). <https://doi.org/10.48550/arXiv.1802.03426> . <https://doi.org/10.48550/arXiv.1802.03426> Accessed 2022-11-13
- [55] Kaya, Y.: Impact of carbon dioxide emission control on GNP growth: interpretation of proposed scenarios. In: IPCC Energy and Industry Subgroup, Response Strategies Working Group (1989)
- [56] Ang, B.W.: The LMDI approach to decomposition analysis: a practical guide. *Energy Policy* **33**(7), 867–871 (2005) <https://doi.org/10.1016/j.enpol.2003.10.010>
- [57] Baldwin, C.Y., Clark, K.B.: The Architecture of Participation: Does Code Architecture Mitigate Free Riding in the Open Source Development Model? *Manage. Sci.* **52**(7), 1116–1127 (2006) <https://doi.org/10.1287/mnsc.1060.0546>
- [58] Krogh, G., Spaeth, S., Lakhani, K.R.: Community, joining, and specialization in open source software innovation: a case study. *Open Source Software Development* **32**(7), 1217–1241 (2003) [https://doi.org/10.1016/s0048-7333\(03\)00050-7](https://doi.org/10.1016/s0048-7333(03)00050-7)
- [59] Verhulst, P.-F.: Notice sur la loi que la population suit dans son accroissement. *Correspondance mathématique et physique* **10**, 113–121 (1838)
- [60] Moradi-Jamei, B., Kramer, B.L., Calderón, J.B.S., Korkmaz, G.: Community formation and detection on GitHub collaboration networks. In: Proceedings of the 2021 IEEE/ACM International Conference on Advances in Social Networks Analysis and Mining. ASONAM '21, pp. 244–251. Association for Computing Machinery, New York, NY, USA (2021). <https://doi.org/10.1145/3487351.3488278> . <https://doi.org/10.1145/3487351.3488278> Accessed 2022-11-08
- [61] Kaplan, E.L., Meier, P.: Nonparametric estimation from incomplete observations. *Journal of the American Statistical Association* **53**(282), 457–481 (1958) <https://doi.org/10.1080/01621459.1958.10501452>
- [62] Cox, D.R.: Regression models and life-tables. *Journal of the Royal Statistical Society. Series B (Methodological)* **34**(2), 187–220 (1972) <https://doi.org/10.1111/j.2517-6161.1972.tb00899.x>
- [63] Coelho, J., Valente, M.T., Milen, L., Silva, L.L.: Is this GitHub project maintained? Measuring the level of maintenance activity of open-source projects. *Information and Software Technology* **122**, 106274 (2020) <https://doi.org/10.1016/j.infsof.2020.106274> . Accessed 2022-11-08
- [64] Moradi Dakhel, A., Majdinasab, V., Nikanjam, A., Khomh, F., Desmarais, M.C., Jiang, Z.M.J.: GitHub Copilot AI pair programmer: Asset or Liability? *Journal of Systems and Software* **203**, 111734 (2023) <https://doi.org/10.1016/j.jss.2023.111734>

- [65] Chen, Z., Jiang, L.: Evaluating Software Development Agents: Patch Patterns, Code Quality, and Issue Complexity in Real-World GitHub Scenarios. In: 2025 IEEE International Conference on Software Analysis, Evolution and Reengineering (SANER), pp. 657–668 (2025). <https://doi.org/10.1109/SANER64311.2025.00068> . ISSN: 2640-7574. <https://doi.org/10.1109/SANER64311.2025.00068> Accessed 2025-09-17
- [66] Vaithilingam, P., Zhang, T., Glassman, E.L.: Expectation vs. Experience: Evaluating the Usability of Code Generation Tools Powered by Large Language Models. In: Extended Abstracts of the 2022 CHI Conference on Human Factors in Computing Systems. ACM, ??? (2022). <https://doi.org/10.1145/3491101.3519665> . <https://doi.org/10.1145/3491101.3519665>
- [67] Pearce, H., Ahmad, B., Tan, B., Dolan-Gavitt, B., Karri, R.: Asleep at the Keyboard? Assessing the Security of GitHub Copilot’s Code Contributions. In: 2022 IEEE Symposium on Security and Privacy (SP), pp. 754–768. IEEE, ??? (2022). <https://doi.org/10.1109/SP46214.2022.9833571> . <https://doi.org/10.1109/SP46214.2022.9833571>
- [68] Tversky, A., Kahneman, D.: Availability: A heuristic for judging frequency and probability. *Cognitive Psychology* **5**(2), 207–232 (1973) [https://doi.org/10.1016/0010-0285\(73\)90033-9](https://doi.org/10.1016/0010-0285(73)90033-9)
- [69] Samuelson, W., Zeckhauser, R.: Status quo bias in decision making. *Journal of Risk and Uncertainty* **1**(1), 7–59 (1988) <https://doi.org/10.1007/BF00055564>
- [70] Sambasivan, N., Arnesen, E., Hutchinson, B., Doshi, T., Prabhakaran, V.: Re-imagining Algorithmic Fairness in India and Beyond. In: Proceedings of the 2021 ACM Conference on Fairness, Accountability, and Transparency. FAccT ’21, pp. 315–328. Association for Computing Machinery, New York, NY, USA (2021). <https://doi.org/10.1145/3442188.3445896> . <https://doi.org/10.1145/3442188.3445896> Accessed 2025-09-17
- [71] Felzmann, H., Villaronga, E.F., Lutz, C., Tamò-Larrieux, A.: Transparency you can trust: Transparency requirements for artificial intelligence between legal norms and contextual concerns. *Big Data & Society* **6**(1), 2053951719860542 (2019) <https://doi.org/10.1177/2053951719860542> . Publisher: SAGE Publications Ltd. Accessed 2025-09-17
- [72] May, R.M.: Will a Large Complex System Be Stable? *Nature* **238**(5364), 413–414 (1972) <https://doi.org/10.1038/238413a0>
- [73] Li, Y., Choi, D., Chung, J., Kushman, N., Schrittwieser, J., Leblond, R., Eccles, T., Keeling, J., Gimeno, F., Dal Lago, A., Hubert, T., Choy, P., Masson d’Autume, C., Babuschkin, I., Chen, X., Huang, P.-S., Welbl, J., Goyal,

- S., Cherepanov, A., Molloy, J., Mankowitz, D.J., Sutherland Robson, E., Kohli, P., Freitas, N., Kavukcuoglu, K., Vinyals, O.: Competition-level code generation with AlphaCode. *Science* **378**(6624), 1092–1097 (2022) <https://doi.org/10.1126/science.abq1158>
- [74] Merchant, A., Batzner, S., Schoenholz, S.S., Aykol, M., Cheon, G., Cubuk, E.D.: Scaling deep learning for materials discovery. *Nature* **624**(7990), 80–85 (2023) <https://doi.org/10.1038/s41586-023-06735-9>
- [75] Mahajan, S., Hausladen, C.I., Argota Sánchez-Vaquerizo, J., Korecki, M., Helbing, D.: Participatory resilience: Surviving, recovering and improving together. *Sustainable Cities and Society* **83**, 103942 (2022) <https://doi.org/10.1016/j.scs.2022.103942> . Accessed 2024-05-23
- [76] Pohle, J., Thiel, T.: Digital sovereignty. *Internet Policy Review* **9**(4) (2020). Accessed 2022-01-13
- [77] Binns, R.: Fairness in Machine Learning: Lessons from Political Philosophy. In: *Proceedings of the 1st Conference on Fairness, Accountability and Transparency*, pp. 149–159 (2018). ISSN: 2640-3498. <https://proceedings.mlr.press/v81/binns18a.html> Accessed 2025-09-17
- [78] Clauset, A., Shalizi, C.R., Newman, M.E.J.: Power-law distributions in empirical data. *SIAM Review* **51**(4), 661–703 (2009) <https://doi.org/10.1137/070710111>

Supplementary Material

Contents

S.1	Bipartite-graph representation and aggregate ecosystem views	p. 32
S.2	Community anatomy: temporal trajectories and size scaling	p. 35
S.2.1	Why single-contributor communities are excluded from the size-scaling fit	p. 35
S.3	Temporal evolution of ecosystem-wide commit activity	p. 36
S.3.1	Multiplicative decomposition of ecosystem-wide annual commits	p. 36
S.3.2	Exploratory unsupervised temporal clustering of communities	p. 39
S.4	Community-scale cross-community coupling	p. 39
S.5	Contributor-scale cross-community structure	p. 41
S.5.1	Diagnostic views of the contributor-breadth distribution	p. 41
S.5.2	Contributor types in the bipartite network	p. 43
S.6	Repository activity forecasting	p. 43
S.7	Community survival: residual phase and hazard predictors	p. 46
S.7.1	Per-community residual phase: time and hazard	p. 46
S.7.2	Predictors of residualisation hazard (static-covariate Cox)	p. 47
S.8	Boundary friction and collaboration depth	p. 50
S.8.1	How boundary friction varies with contributor breadth k	p. 50

S.1 Bipartite-graph representation and aggregate ecosystem views

This section assembles the figures that establish the data substrate of the study: the cybersecurity OSS ecosystem viewed as a single bipartite contributor–repository graph, the longitudinal community-level metrics that motivate the per-community treatment in Figure 2A, and the comparison of the bipartite representation against its unipartite projections that motivates working with the bipartite graph directly throughout Methods and Results.

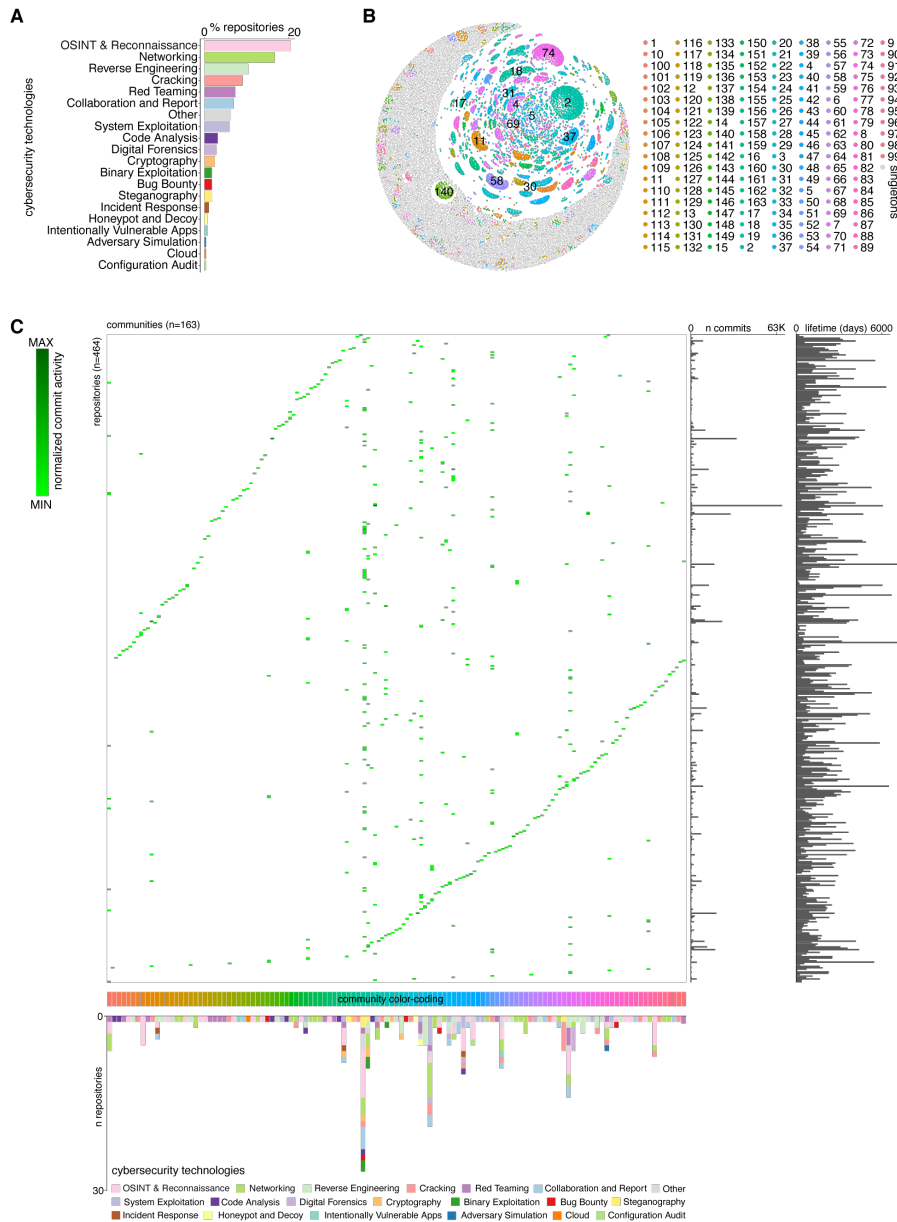


Fig. S1 Activity patterns and representation of OSS Technologies and Communities under study. **A.** Barplot illustrating the representation of cybersecurity technologies in the OSS ecosystem under study: percentage of repositories by technology subtype. **B.** Scatter plot depicting coordinates of Bipartite network built on commit relationships between contributors and repositories [historical aggregate] color-coded by identified communities. Numerical ID and color-coding associated with each community is detailed in legend. Bigger communities are highlighted in network by displaying their IDs. **C.** Heatmap illustrating the normalized commit activity of each repository and associated community: number of commits divided by repository lifetime [color gradient: light-green (relative low normalized activity) to dark-green (relative high normalized activity)]. Y-axis joint barplots indicate counts of number of commits and repository lifetime. X-axis joint barplot indicates composition of technologies for each community [technology color-coding as in A., community color-coding as in B.].

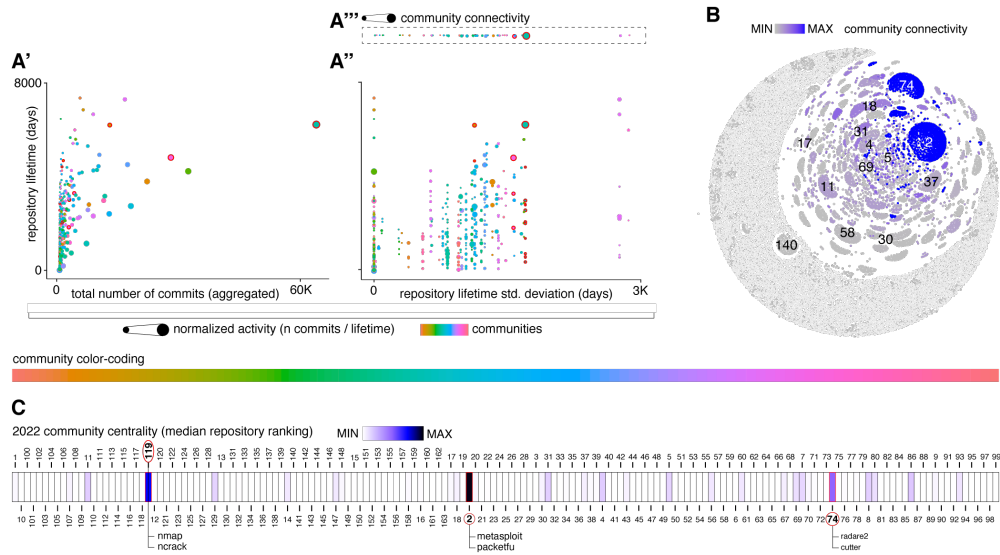


Fig. S2 Community Lifetime, Connectivity and Centrality. **A'**. Scatter plot depicting repositories ordered by their total number of commits through time (y-axis) and their lifetime in days (y-axis; days of activity). Color-coding groups repositories by community belonging [rainbow discrete palette from orange to pink]. Dot size indicates repository normalized activity (total number of commits divided by lifetime) **A''**. Scatter plot depicting repositories ordered by their lifetime standard deviation [variation in days between commit activity registry] (x-axis) and their lifetime in days (y-axis; days of activity). Color-coding groups repositories by community belonging [rainbow discrete palette from orange to pink]. Dot size indicates repository normalized activity (total number of commits divided by lifetime) **A'''**. Scatter plot depicting repositories ordered by their lifetime standard deviation [as in **A''** x-axis] and sized by their inter community connectivity. In **A'**, **A''**, and **A'''**, red-contoured dots correspond to repositories whose community is among the top-3 centrality in 2022 network. **B**. Bipartite network scatter plot color-coded by community inter connectivity [gradient scale: grey (low inter connectivity) to blue (high inter connectivity)]. ID highlighted communities: biggest in terms of contributors and / or highest in terms of commit activity. **C**. Heatmap color-coded by centrality score of communities as of 2022 aggregated network [gradient scale: grey (low centrality) to blue (high centrality)]. Red-contoured fields correspond to repositories whose community is among the top-3 centrality. For those, top 2 centrality repositories are indicated.

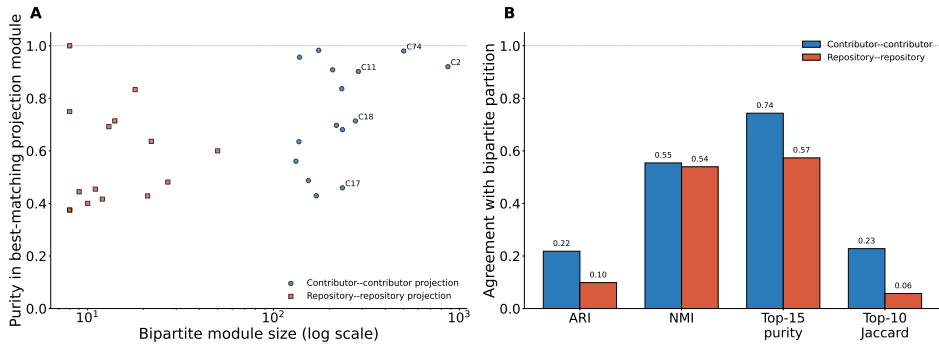


Fig. S3 Information content of the bipartite representation. The community structure reported in Results on the bipartite graph $G = (U, V, E)$ is not recoverable from unipartite projections of G . **A.** Per-community purity versus community size for the 15 largest bipartite communities, under the contributor-contributor projection [edge weight = number of shared repositories; blue circles] and the repository-repository projection [edge weight = number of shared contributors; orange squares]: large bipartite communities are partially preserved on the contributor side (mean purity 0.74) but substantially collapsed on the repository side (mean purity 0.57). **B.** Aggregate agreement with the bipartite partition [adjusted Rand index, normalised mutual information, mean top-15 purity, mean top-10 Jaccard] for the contributor-contributor and repository-repository projections. The combined evidence quantifies the information loss that motivates using the bipartite representation directly as the object of inference [52, 53], rather than a one-mode projection of it.

S.2 Community anatomy: temporal trajectories and size scaling

This section supports Figure 2B of the main text by justifying the singleton exclusion in the size-scaling fit.

S.2.1 Why single-contributor communities are excluded from the size-scaling fit

The OLS power-law fit reported alongside Figure 2B uses the 124 non-singleton Louvain communities for which $n_{\text{contributors}} > 1$, and excludes the 39 communities for which $n_{\text{contributors}} = 1$. The exclusion is principled rather than aesthetic. The quantity that the fit characterises is how many contributors a community accrues as it accrues repositories, and that scaling is undefined for a community whose contributor count is fixed at one regardless of n_{repos} : 38 of the 39 excluded points sit at the corner $(n_{\text{repos}}, n_{\text{contributors}}) = (1, 1)$ and the remaining one at $(2, 1)$, so the excluded subset encodes no within-community contributor-pair collaboration and is a degenerate strip rather than the lower tail of a distribution. We retain the singletons in the panel as small open grey markers for visual completeness only.

S.3 Temporal evolution of ecosystem-wide commit activity

This section quantifies the per-community temporal heterogeneity visible in Figure 2A through a multiplicative (Kaya-style) decomposition of ecosystem-wide annual commits into an extensive and an intensive margin, and reports an exploratory unsupervised clustering of the per-community trajectories that does not enter the main analytical narrative.

S.3.1 Multiplicative decomposition of ecosystem-wide annual commits

The qualitative observation in Figure 2A – “more communities, less steady contributions” – has a clean quantitative analogue obtained by decomposing the ecosystem-wide annual commit total into an extensive and an intensive margin. Let $T(y) = \sum_c a_c(y)$ be total annual commits, $N(y) = \#\{c : a_c(y) > 0\}$ the number of active communities in year y , and $\bar{e}(y) = T(y)/N(y)$ the mean commits per active community. By construction $T(y) = N(y)\bar{e}(y)$, so taking logs and first differences yields a Kaya-style identity [55, 56]

$$\Delta \log T(y) = \Delta \log N(y) + \Delta \log \bar{e}(y),$$

i.e. each year’s growth rate of total commits is exactly the algebraic sum of the growth rate of the active-community count and the growth rate of mean per-community commits. We additionally fit a three-parameter logistic to the cumulative-births series $N_{\text{born}}(y) = \#\{c : b_c \leq y\}$ via `scipy.optimize.curve_fit`, recovering a carrying capacity K , an intrinsic growth rate r , and an inflection year t_0 . We split the time series at $\lfloor t_0 \rfloor$ and report the cohort-mean values of $\Delta \log N$, $\Delta \log \bar{e}$, and $\Delta \log T$ over each window. Mean per active community is plotted on its own logarithmic twin axis in Figure S4B.1 [rather than co-plotted on the same logarithmic axis as $T(y)$] so that its ~ 1 -decade dynamic range is not visually compressed against the ~ 4 -decade dynamic range of the total.

The logistic fit to cumulative births returns $K = 251.9$ communities, $r = 0.276 \text{ yr}^{-1}$, and $t_0 = 2018.45$, consistent with the values reported on the same full-calendar-year window in the main text (Figure 2A). Mean commits per active community peaks earlier, in 2014, at $\bar{e} = 1,038$ commits per community per year, then declines monotonically. The two regime means are summarised in Table S1. Pre- t_0 , the active-community count contributes 96% of total growth [0.282/0.294], while per-community intensity is essentially flat [+0.012 yr⁻¹]; post- t_0 , the per-community decline contributes 84% of the total drop [-0.065/-0.077], while the active-community count is roughly stationary. Two distinct inflections are therefore visible: a per-community level inflection near 2014 [the peak of \bar{e}], and a births-rate inflection at $t_0 \approx 2018.5$ [the inflection of the logistic fit to N_{born}]. Between 2014 and 2018, \bar{e} is already declining but N_{born} is still increasing – the dormant gap between N_{born} and N_{active} [light-teal fill in Figure S4B.1] widens visibly post-2014, indicating that some of the new births contribute zero commits in a given year and so N_{active} lags N_{born} .

Table S1 Regime-mean year-on-year log-decomposition of ecosystem-wide annual commits, split at the logistic-births inflection $\lfloor t_0 \rfloor = 2018$.

period	mean $\Delta \log N$	mean $\Delta \log \bar{e}$	mean $\Delta \log T$
2002–2018 [pre- t_0]	+0.282 yr ⁻¹	+0.012 yr ⁻¹	+0.294 yr ⁻¹
2019–2021 [post- t_0]	-0.011 yr ⁻¹	-0.065 yr ⁻¹	-0.077 yr ⁻¹

The decomposition recasts the “more communities, less steady” pattern as a two-regime story. Until 2014, the ecosystem grows because new communities are being added at high rate while established communities sustain their per-year intensity; both terms are positive but $\Delta \log N$ dominates. Between 2014 and 2018, per-community intensity has already begun to fall, but births are still numerous enough that the total keeps rising and the aggregate masks an internal shift. After 2018, the logistic-saturated births can no longer offset the persistent per-community decline, and the ecosystem total turns negative, driven almost entirely by the intensive margin. The four-year lag between the per-community peak and the births inflection is the key signature: a manager reading only $T(y)$ would have missed the per-community decline for ~ 4 years, since the births inflow was hiding it. In a maturing open-source ecosystem, the first sign of regime change is in the intensive margin (\bar{e}), not the extensive one (N). A caveat is that $N(y)$ is here defined as “ ≥ 1 commit in year y ”, a binary activity flag that gives equal weight to a community with one commit and one with thousands; a robustness re-run with $N^{(k)}(y) = \#\{c : a_c(y) \geq k\}$ for $k \in \{5, 50\}$ would tell us whether the 2014 per-community peak reflects a genuine shift in established-community behaviour or an influx of nominally-active communities that drag the mean down.

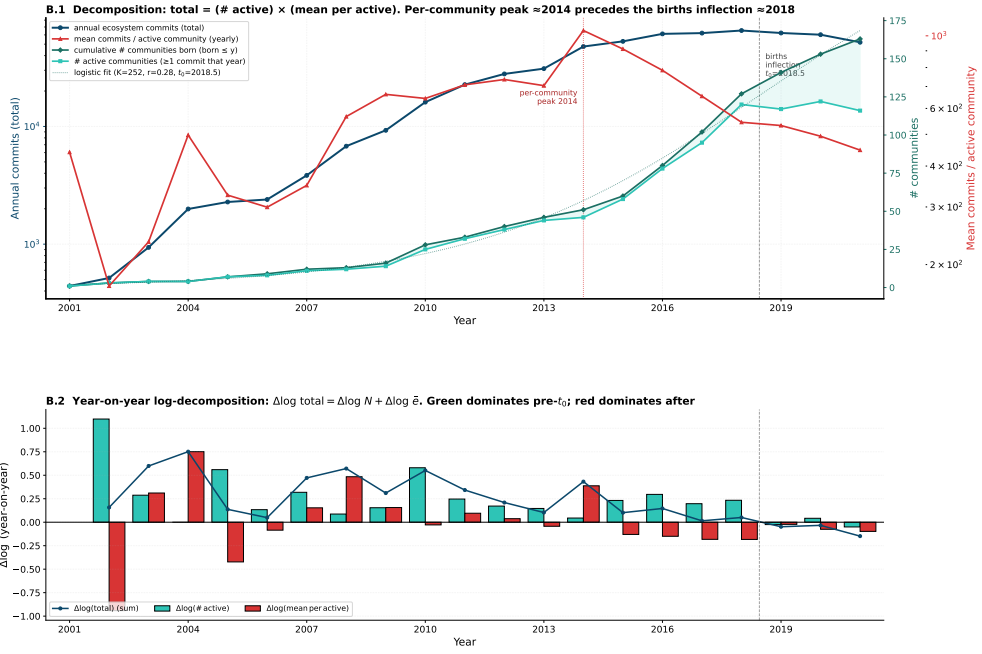


Fig. S4 Multiplicative decomposition of ecosystem-wide annual commits. Aligned x -axis (2001–2021) for both panels. **B.1.** Annual ecosystem commits $T(y)$ [blue, left log axis], mean commits per active community $\bar{e}(y) = T(y)/N(y)$ [red, right log axis], and the cumulative number of communities born $N_{\text{born}}(y)$ [dark teal] and active $N(y)$ [light teal] on a shared linear axis, with a logistic fit ($K = 252, r = 0.28, t_0 = 2018.5$) to $N_{\text{born}}(y)$. The light-teal fill marks the dormant gap [born but inactive that year]. Two inflections are annotated: the per-community peak ≈ 2014 [vertical dotted red] and the births inflection $t_0 \approx 2018.5$ [vertical dashed grey]. **B.2.** Year-on-year log decomposition $\Delta \log T = \Delta \log N + \Delta \log \bar{e}$. Green bars: contribution from the change in the active-community count. Red bars: contribution from the change in mean commits per active community. Blue line: their algebraic sum, equal to the year-on-year growth rate of total commits. Pre- t_0 growth is carried by green bars; post- t_0 decline is carried by red bars. Regime means are reported in Table S1.

S.3.2 Exploratory unsupervised temporal clustering of communities

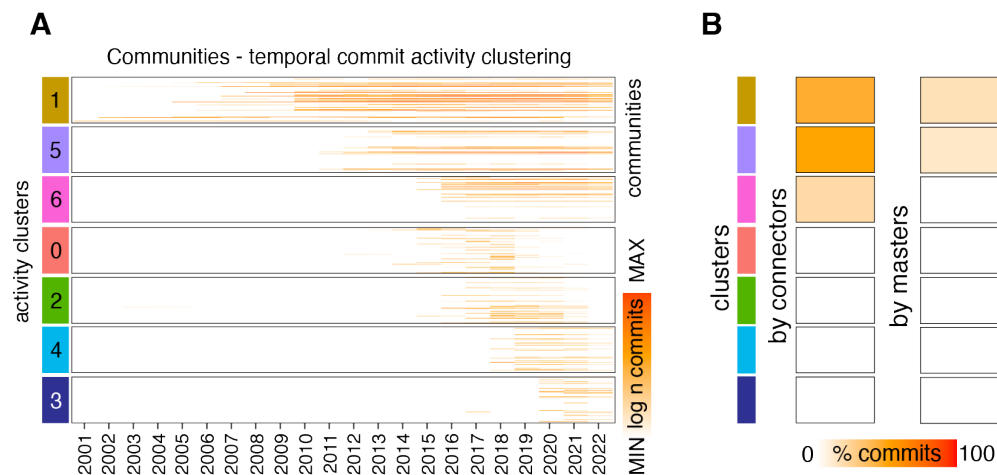


Fig. S5 Exploratory unsupervised temporal clustering of communities (not used in the main text). **A.** Heatmap stack, one per cluster, detailing log-transformed annual commit activity for each non-singleton Louvain community [rows] over 2001–2022 [columns]; cluster colour-coding shown at the left margin. The pipeline uses Seurat-style normalisation, PCA, UMAP on the leading components, and Louvain-type clustering on the resulting two-dimensional embedding [Methods Section 3]. A pairwise adjusted Rand index of 0.51 across $n_{\text{neighbors}} \in \{5, 15, 30\}$ indicates that the cluster boundaries are not robust to local-connectivity choices, and the same temporal heterogeneity is now visualised in the main text as a per-community heatmap sorted by birth year (Figure 2A). **B.** Distribution of commit shares attributable to contributors with $k \geq 5$ and $k \geq 10$ repositories, by temporal cluster [this figure was produced before the present analysis adopted the data-driven $k \geq 7$ cross-community contributor threshold, so the legacy bins are kept here for visual reference only]: high- k contributors tend to concentrate in sustained-engagement clusters, an observation that resurfaces in the main text under a continuous, contributor-level lens (Figure 3C–D).

S.4 Community-scale cross-community coupling

This section supports Figure 3A–B of the main text by reporting the community-level activity-versus-coupling association and an exploratory clustering of communities along an event-ratio axis.

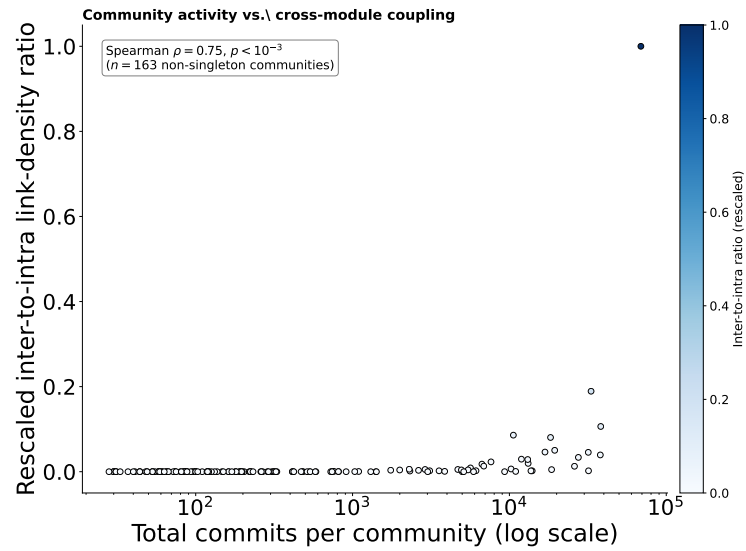


Fig. S6 Community-level activity versus cross-community coupling. Per-community total commits [x -axis, log scale] versus rescaled inter-to-intra link-density ratio [y -axis], across the 163 non-singleton Louvain communities. Total commits and the rescaled inter-to-intra ratio are positively rank-correlated (Spearman $\rho \approx 0.75$, $p < 10^{-3}$): communities with higher total commit volumes consistently exhibit higher cross-community coupling. The same association is unpacked at finer granularity in the main text via the depth-of-collaboration analysis [Section 4.5, Figure 5].

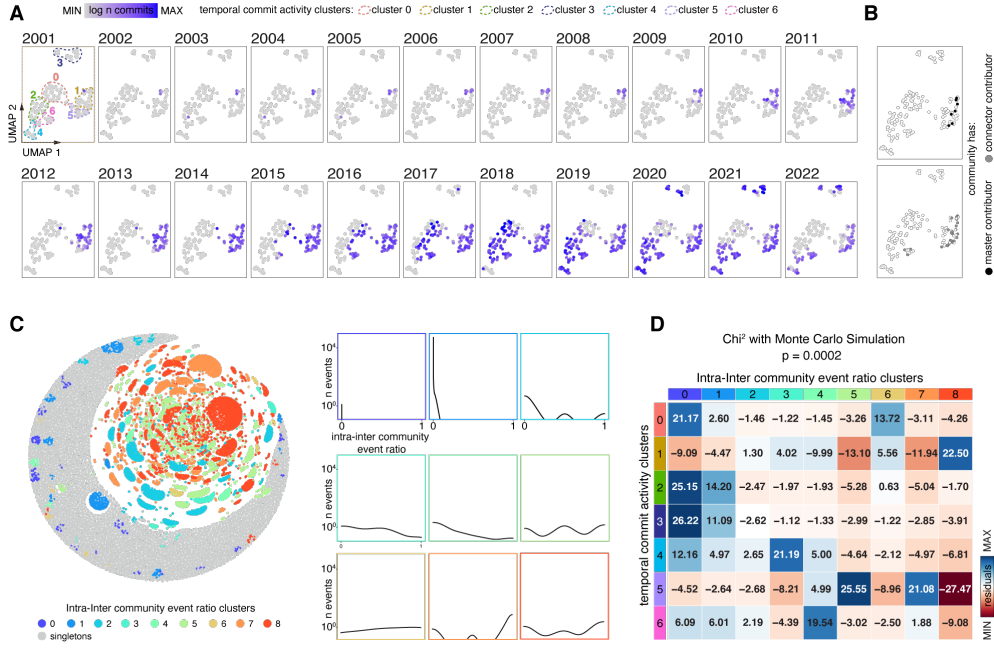


Fig. S7 Community Temporal clustering, Event Ratio clustering, Clustering Association. **A.** Grid of yearly scatter plots illustrating UMAP positioning of communities by their pattern of temporal activity [community temporal clustering]. First scatter on the grid highlights cluster boundaries and labels. Color-coding of UMAP scatter plots indicate the log number of commits made at each year by each community. **B.** Scatter plots with UMAP community temporal activity coordinates highlighting communities that host contributors with $k \geq 5$ [grey, top] and $k \geq 10$ [black, bottom] repositories [the figure pre-dates the data-driven $k \geq 7$ cross-community contributor threshold of the current analysis and is kept here only for the legacy comparison]. **C.** (left) OSS Activity Network color coding contributors as by their event ratio clustering labels. (right) Grid line plots split by event ratio clusters showing the relation between number of events each contributor is associated to and their positioning in the intra-inter community event ratio score. Color-coding is included in left side legend and in line plot outline. **D.** Heatmap showing the Chi-squared residuals for the association test examining the relation between the two types of clustering covered in this figure: temporal commit activity clusters [y-axis] and event ratio clusters [x-axis]. Color-coding from brown (negative residuals) to blue (positive residuals).

S.5 Contributor-scale cross-community structure

This section supports Figure 3C–D of the main text by reporting the diagnostic views (CCDF and SSR scan) that justify the two-regime fit on the contributor-breadth distribution, and a complementary contributor-typology view used in earlier work.

S.5.1 Diagnostic views of the contributor-breadth distribution

The main-text Figure 3C shows the empirical PMF of contributor breadth k together with an adaptive Abramson KDE and a two-regime OLS fit whose breakpoint $k^* = 7$ is chosen by minimising body+tail SSR. Figure S8 reports the two diagnostic views that motivate that choice. **Panel A** plots the empirical CCDF of k on log–log axes together with a single discrete power-law fit to the multi-community subset ($k \geq 2$), estimated by the Hurwitz-zeta MLE of [78]. The MLE returns a CCDF exponent

$\mu = \alpha - 1 = 3.00$ [95% non-parametric bootstrap CI [2.80, 3.22], $B = 1,000$ resamples]. The fit captures the body of the distribution but underestimates the upper tail: the nine humans at $k \geq 7$ sit visibly above the predicted CCDF, indicating that a single power law is too restrictive a model for the full range of k . **Panel B** reports the SSR scan that selects the two-regime breakpoint used in the main text. For each candidate $k^* \in [3, 14]$ we fit a power law to the body ($k < k^*$) and to the tail ($k \geq k^*$) by OLS on $\log_{10} k$ versus \log_{10} PMF, summing the body and tail squared residuals. Open circles mark candidates with at least five unique tail k values [eligible for selection]; grey squares mark candidates with fewer unique tail points [shown for completeness; an OLS fit on a tail of two or three points achieves a trivially low SSR by interpolation, so these are not eligible]. The total SSR drops sharply from 0.58 at $k^* = 6$ to 0.13 at $k^* = 7$ – the elbow that defines the data-driven breakpoint – and stays in the range 0.11–0.14 for all $k^* \geq 7$, including the ineligible ones: every candidate that places at least one of the high- k humans inside the tail yields essentially the same residual, confirming that $k = 7$ is the latest defensible position for the breakpoint.

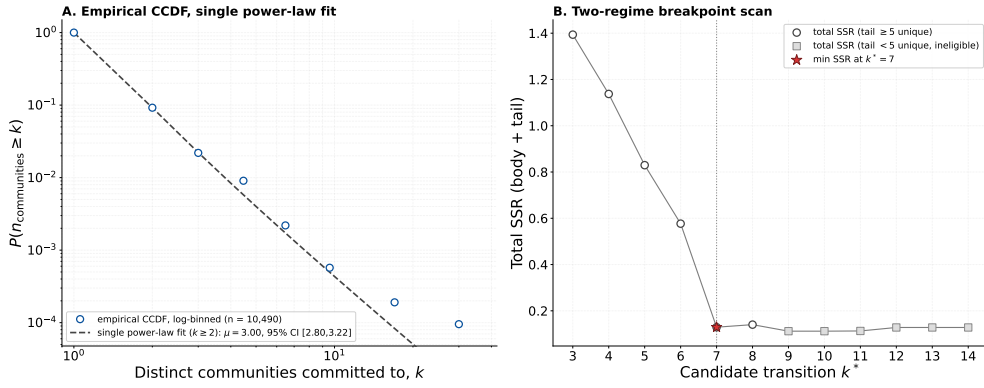


Fig. S8 Diagnostic views supporting the two-regime fit in Figure 3C. **A.** Empirical CCDF of contributor breadth k on log–log axes [open blue circles, $n = 10,490$ canonical human contributors after bot/phantom removal], log-binned for legibility into eight bins of equal width on $\log_{10} k$: each circle is plotted at the geometric mean of the observed integer k values in its bin, with y equal to the empirical CCDF evaluated at the smallest of those k values [preserving the $P(X \geq k)$ semantic]. The dashed grey line is a single discrete power-law fit on the multi-community subset $k \geq 2$ [Hurwitz-zeta MLE]. The single-fit CCDF exponent is $\mu = \alpha - 1 = 3.00$ [95% bootstrap CI [2.80, 3.22], $B = 1,000$]. The nine humans at $k \geq 7$ lie above the fitted CCDF, so a single straight line is insufficient to describe the upper tail. **B.** Sum of squared residuals [body+tail OLS in log–log space on the empirical PMF] as a function of the candidate transition k^* . Open circles are eligible candidates [tail has ≥ 5 unique k values]; grey squares are ineligible [tail < 5 unique k]. The red star marks the min-SSR breakpoint $k^* = 7$ used in the main text. The sharp drop from 0.58 at $k^* = 6$ to 0.13 at $k^* = 7$ is the elbow that defines the data-driven inflection.

of commit activity as a feature [capturing auto-regressive memory in addition to all structural features]; *Model 2* excludes the recent-history feature, which isolates the structural contribution of community membership and cross-community exposure from short-run persistence. Variable importance is reported as percentage increase in mean squared error under feature permutation; prediction error is the per-repository residual on the holdout. The headline observation – that ecosystem embedding [number of community links, inter-/intra-community PR ratio, repository-level link-density summaries, lifetime] retains substantial explanatory power once recent history is removed – complements the contributor-scale story: the structural substrate identified at the contributor scale is observable enough at the repository scale to forecast future activity.

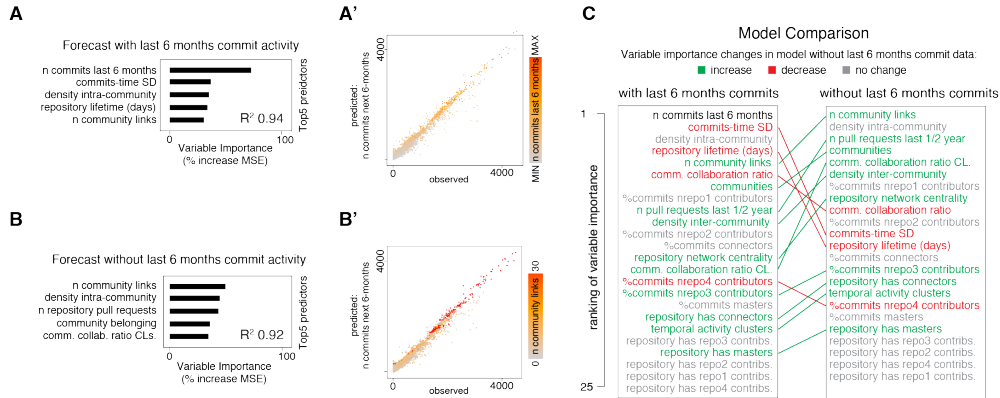


Fig. S10 Repository six-month commit-volume forecasting under structural-vs-temporal ablation. **A.** Variable-importance ranking for Model 1 [with the previous six months of commit activity included]: ranking is by percentage increase in MSE under feature permutation, with the per-feature standard error of the predicted commit count on the x -axis. **A'.** Per-repository observed-vs-predicted scatter for Model 1; colour encodes the previous six months of commits [the dominant predictor]. **B.** Variable importance for Model 2 [recent-history feature removed]: the number of community links and the inter-/intra-community PR ratio rise to the top of the ranking. **B'.** Observed-vs-predicted scatter for Model 2; colour encodes the number of community links per repository [the dominant predictor in this model]. **C.** Cross-model variable-importance comparison: variables are listed in order of importance per model, and the connecting links indicate whether each variable's importance dropped (red), increased (green), or held (grey) when the recent-history feature was removed. The persistence of community-link and inter-/intra-community-ratio importance under the ablation is the principal forecast-side evidence for the ecosystem-embedding claim made in Section 4.5.

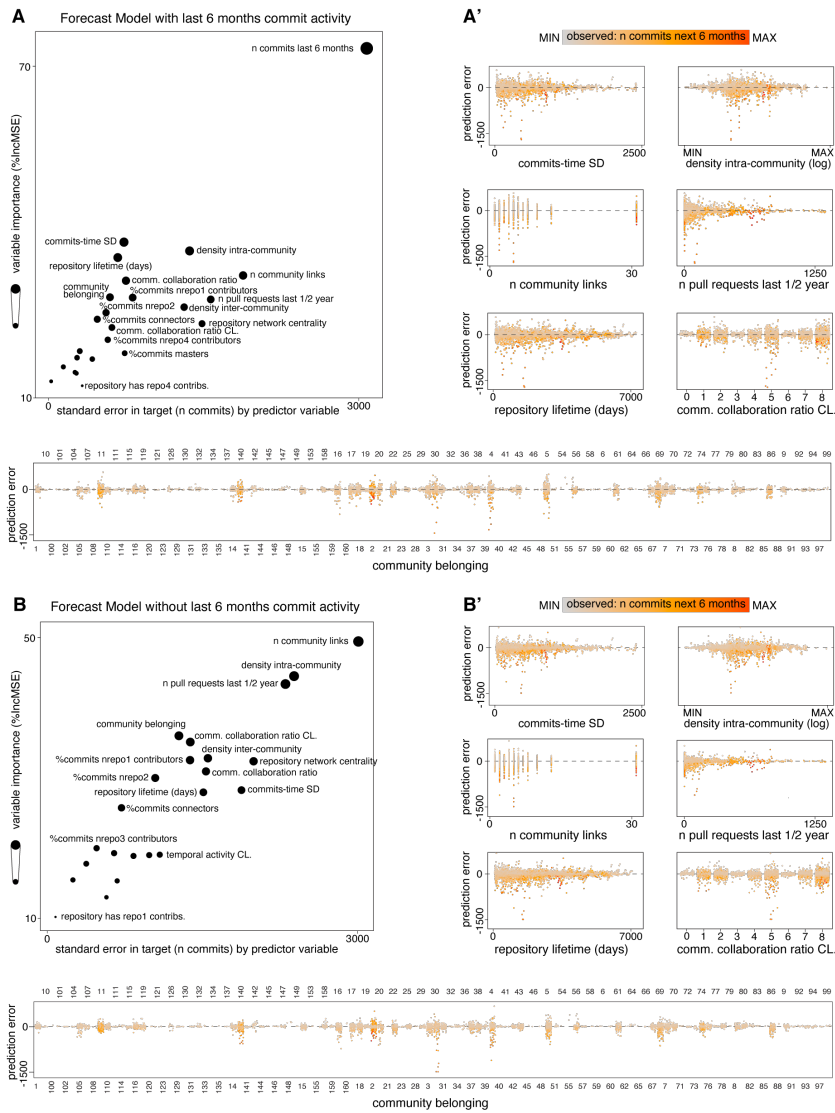


Fig. S11 Forecast modeling performance comparison. **A.** Variable importance for Model 1 [with the previous six months of activity], with each variable's percentage increase in MSE under permutation on the y -axis and dot size, and the standard error of the predicted commit count on the x -axis. **A'.** Top predictive variables for both models with their per-repository prediction error on the y -axis, coloured by the observed next-6-month commit count. **B.** Variable importance for Model 2 [recent history excluded], same axes as panel A. **B'.** Top predictive variables for both models with prediction error coloured by observed next-6-month commit count.

S.7 Community survival: residual phase and hazard predictors

This section supports the community-survival analysis in the main text (Figure 4, Table 1). We first define the residual-phase outcome, the per-cohort annual hazard, and report the cohort-structured time-to-residual pattern; we then test whether community-level features beyond cohort and size predict residualisation, with full Cox proportional-hazards diagnostics.

S.7.1 Per-community residual phase: time and hazard

Figure 2A shows that the earliest cohorts of communities sustain multi-year contribution streaks, while later cohorts appear less steady. We quantify that observation here as a residual-phase analysis. For each non-singleton Louvain community c , let $a_c(y)$ be the number of commits to c in calendar year y , taken from `commit_pr_timedata.csv` with author/repository community labels from the bipartite Louvain partition (`out/BiNet/g_full.csv`). The observation horizon is set to the last full year of GitHub Archive coverage in our window, $Y_{\text{end}} = 2021$; the partial 2022 window is excluded from rate-based statistics. We define the community’s birth year as $b_c = \min\{y : a_c(y) > 0\}$, its mean yearly activity as

$$\mu_c = \frac{1}{Y_{\text{end}} - b_c + 1} \sum_{y=b_c}^{Y_{\text{end}}} a_c(y),$$

and a residual threshold $\theta_c = 0.05 \mu_c$. The last non-residual year is $y_c^* = \max\{y \in [b_c, Y_{\text{end}}] : a_c(y) \geq \theta_c\}$, and the non-residual span [Figure 4A, y -axis] is $y_c^* - b_c + 1$ years. A community is right-censored if $y_c^* = Y_{\text{end}}$ – the observation window terminates while the community is still above threshold. The per-cohort annual hazard rate [Figure 4A'] is computed as

$$h(\text{cohort}) = \frac{\#\{\text{events in cohort}\}}{\sum_{c \in \text{cohort}} (y_c^* - b_c + 1)},$$

i.e. the empirical mean annual transition probability into residual conditional on still being non-residual. The hazard formulation is preferred over a cumulative-event share or a mean time-to-residual because it normalises by the time the cohort has actually been observed at risk; raw event shares would bias early cohorts upward [longer observation] and late cohorts downward [truncated by the censoring envelope $Y_{\text{end}} - b_c + 1$, shown as the dashed line in Figure 4A].

Across the 163 non-singleton communities, 55 have entered the residual phase by 2021 and 108 are right-censored. The median time-to-residual is 5 years overall, but the distribution is strongly cohort-structured. Communities born in 2001–2010 sit close to the censoring envelope, indicating that they are still active above 5% of their long-run mean after 11–20 years; communities born in 2011–2014 show a mixed pattern split between censored and 3–7-year non-residual spans; communities born in 2015–2021 are sharply bimodal between very short [≤ 3 -year] non-residual spans and a tail of censored cases reflecting their truncated observation windows. The colour scale [mean yearly

commits] shows that the surviving [censored] communities are systematically higher-volume; small communities are over-represented among events. The per-cohort hazard [Figure 4A'] makes the cohort effect explicit: pre-2010 cohorts sit at 0–0.05 yr⁻¹, then the hazard rises sharply for the 2015–2018 cohorts, peaking at 0.193 yr⁻¹ for the 2018 cohort [$n = 25$]. The 2019–2021 cohorts have lower observed hazards, but those are small-sample [cohort sizes $n = 14, 12, 10$] and bounded above by the limited time available since their birth.

Two distinct mechanisms compound in this cohort effect. The first is a geometric ceiling: a community born in 2018 cannot, by construction, accumulate more than 4 years of non-residual life by 2021, and the censoring envelope in Figure 4A makes this constraint explicit. The hazard formulation in Figure 4A' normalises by years-at-risk and is therefore not mechanically driven by this. The second is genuine cohort heterogeneity: even after the time-at-risk normalisation, the hazard rises by roughly an order of magnitude between the pre-2010 cohorts [~ 0.02 – 0.05 yr⁻¹] and the 2015–2018 cohorts [0.10 – 0.19 yr⁻¹], so communities born after the community-count peak transition [Figure 2A, ~ 2017] are intrinsically more likely to drop into residual within any given year. The mean-yearly-commits colour mapping suggests a complementary point: late cohorts that do survive tend to be smaller, while the highest-volume late entrants are also the ones most likely to remain censored, so volume is a precondition for sustained activity but not a sufficient one for the early cohorts [which can persist on small but continuous activity]. The 5%-of-mean-yearly threshold is conservative for communities with long dormant tails; sensitivity analyses with thresholds at 1% and 10% of mean yearly are not reported here but should be checked before any policy claim is built on the per-cohort hazard.

The visual companions to this section – the time-to-residual scatter and the per-cohort hazard bars – are reported in the main text as panels A and A' of Figure 4.

S.7.2 Predictors of residualisation hazard (static-covariate Cox)

The headline numbers from this section are reported in the main text as Figure 4 and Table 1. This subsection retains the full Cox proportional-hazards diagnostic [univariate and multivariate model fits, two Kaplan–Meier stratifications, and the static-window caveats] for readers who want the underlying detail.

Section S.7.1 established that the per-cohort hazard rate of entering residual rises by an order of magnitude between pre-2010 cohorts and the 2015–2018 cohorts. A natural follow-up is whether community-level features beyond birth year predict residualisation, and in particular whether *insufficient cross-community connectivity* – the structural feature emphasised throughout this paper – is associated with higher hazard once cohort and size are controlled for. We test the hypothesis with a Cox proportional-hazards (PH) model on the same 163 communities and the same outcome [time-to-residual through 2021, with right-censoring] used in Section S.7.1.

Cox PH and Kaplan–Meier in a nutshell.

Both are tools for time-to-event data with right-censoring. The Kaplan–Meier (KM) estimator is non-parametric: it estimates the survival function $S(t) =$

\mathbb{P} (community still non-residual at age t) by walking through event times and updating S at each by the conditional surviving fraction. Stratified KM splits the cohort into groups and renders one curve per stratum; a multi-group log-rank test compares the curves under a no-difference null. Cox PH is the regression workhorse:

$$h(t | \mathbf{x}) = h_0(t) \exp(\beta_1 x_1 + \beta_2 x_2 + \dots),$$

where the baseline hazard $h_0(t)$ is left unspecified and only the multiplicative effect of the covariates is estimated. The hazard ratio $\text{HR} = \exp(\beta)$ is the per-unit multiplier of the per-year residualisation risk: $\text{HR} > 1$ accelerates the event, $\text{HR} < 1$ is protective. The proportional-hazards assumption requires that the ratio $h(t | \mathbf{x}_a)/h(t | \mathbf{x}_b)$ does not change with t . Concordance C is a discrimination measure: the probability that for a random pair where one community failed earlier, the model assigned it a higher hazard [$C = 0.5$ chance, $C = 1$ perfect].

Per-community predictors.

For each community c we assemble three classes of covariates from the end-of-window snapshot. *Cohort and size* [controls]: birth year b_c ; \log_{10} number of repositories from `df_commrepo.csv`; \log_{10} number of distinct contributors. *Cross-community PR connectivity*: the inter-community PR share

$$\text{inter-share}_c = \frac{n_c^{\text{inter}}}{n_c^{\text{intra}} + n_c^{\text{inter}}},$$

where n_c^{intra} [n_c^{inter}] is the number of pull-requests opened by an author whose home community is [is not] the repository’s community, taken from `out/revision/figure_cross_community/per_community_pr.csv`. *Cross-community contributor structure*: the share of c ’s contributors who have committed to ≥ 2 Louvain communities (`cross_share_k2`); and the network-degree measure $\log_{10}(1+d_c^{\text{ext}})$, where d_c^{ext} is the number of *other* communities that either send commits into c or receive commits from c ’s home contributors – the symmetric inter-community degree of c in the cross-commit graph.

Modelling.

We fit Cox PH models with `lifelines.CoxPHFitter`, taking time-to-residual [years from birth] as the duration and event = 1 – censored as the indicator. Univariate models report a single-predictor HR, 95% Wald CI, p -value and concordance index. The multivariate model uses cohort + size + a parsimonious set of connectivity covariates. We also fit Kaplan–Meier survival curves stratified by tertiles of two key cross-community measures, with multi-group log-rank tests.

Results.

Univariately, every cohort and size variable is highly significant: birth year [HR= 1.38 per year, $p < 10^{-3}$, $C = 0.73$]; \log_{10} # contributors [HR= 0.17, $p < 10^{-3}$, $C = 0.80$]; \log_{10} # repositories [HR= 0.011, $p < 10^{-3}$, $C = 0.68$]; \log_{10} total commits [HR=

0.23, $p < 10^{-3}$, $C = 0.79$]. Among the cross-community measures, the strongest univariate predictor is the external-community degree $\log_{10}(1 + d_c^{\text{ext}})$ [HR= 0.072, 95% CI [0.030, 0.174], $p < 10^{-3}$, $C = 0.77$]: a one-decade increase in the number of other communities reached cuts the residualisation hazard by a factor of ~ 14 . The number of inter-community PRs is similarly protective [$\log_{10}(1 + n_c^{\text{inter}})$: HR= 0.15, $p < 10^{-3}$]. The inter-community PR *share* is not significant univariately [HR= 0.67, $p = 0.62$], reflecting the fact that very small communities can have a high inter-share by accident of having a single boundary-crossing PR; only after size is controlled for does the share become an interpretable predictor.

The multivariate model [Table S2, Figure S12] achieves concordance $C = 0.843$. After controlling for cohort and size, three observations bear directly on the hypothesis. First, birth year remains an independent predictor [HR= 1.18, $p = 0.021$]: the cohort effect is real and not fully explained by community size or connectivity. Second, \log_{10} # contributors retains a borderline-significant protective signal [HR= 0.39, $p = 0.055$]; \log_{10} # repositories is no longer significant [$p = 0.29$] because contributor count and repo count are highly collinear. Third – the test – the inter-community PR share is significantly protective once size is controlled for: HR= 0.11 [95% CI [0.02, 0.61], $p = 0.012$]. A community whose PR mix is one full unit [i.e., 0 to 100%] more cross-community has roughly a tenfold lower instantaneous hazard than a same-cohort, same-size community whose PRs are predominantly intra-community.

Table S2 Multivariate Cox proportional-hazards model of community residualisation [n=163, events=55, concordance $C = 0.843$]. HRs are per unit of the listed predictor on the original scale (years for birth year, \log_{10} units for log-transformed predictors, fraction for shares).

predictor	HR	95% CI lower	95% CI upper	p
Birth year	1.18	1.03	1.35	0.021
\log_{10} # repositories	0.21	0.01	3.87	0.292
\log_{10} # contributors	0.39	0.15	1.02	0.055
Inter-community PR share	0.11	0.02	0.61	0.012
\log_{10} # external communities reached	0.19	0.02	2.09	0.176
Share of contributors ≥ 2 communities	4.72	0.39	56.6	0.221

The two Kaplan–Meier stratifications corresponding to the same cross-community measures are reported in the main text as panels B and C of Figure 4. Stratifying by inter-community PR share gives a multi-group log-rank statistic of $\chi^2 = 21.9$, $p = 1.8 \times 10^{-5}$: the high-share tertile sustains a ~ 0.55 probability of remaining non-residual at 10 years from birth versus ~ 0.30 for the low-share tertile. Stratifying by external-community degree gives a sharper separation [$\chi^2 = 49.1$, $p = 2.2 \times 10^{-11}$]: communities in the highest tertile of external reach have a ~ 0.95 ten-year non-residual probability against ~ 0.10 for the lowest tertile [in the multivariate model the same predictor attenuates to HR= 0.19, $p = 0.18$, partly mediated by community size].

Caveats.

All predictors here are end-of-window summaries computed on the aggregate corpus, and three caveats apply. First, the inter-community PR share is itself correlated with birth year [Spearman $\rho = -0.21$, $p = 0.006$ on all 163 communities; $\rho = -0.32$, $p = 0.005$ restricted to those with ≥ 50 PRs]: late cohorts have less time to accumulate PR history and many have no PRs at all [40% of the 2021 cohort], inflating the cohort signal. Second, the proportional-hazards assumption is not formally tested here [Schoenfeld residuals]; the strong cohort effect makes it plausible that hazards are not strictly proportional across cohorts. Third, the static-covariate framing creates an obvious reverse-causation concern: a community already approaching residual may attract fewer external PRs because it is already perceived as inactive, so the protective association observed at end of window may partly be an effect of survival rather than its cause. The static results reported here should therefore be read as descriptions of end-of-window association rather than as causal-direction tests.

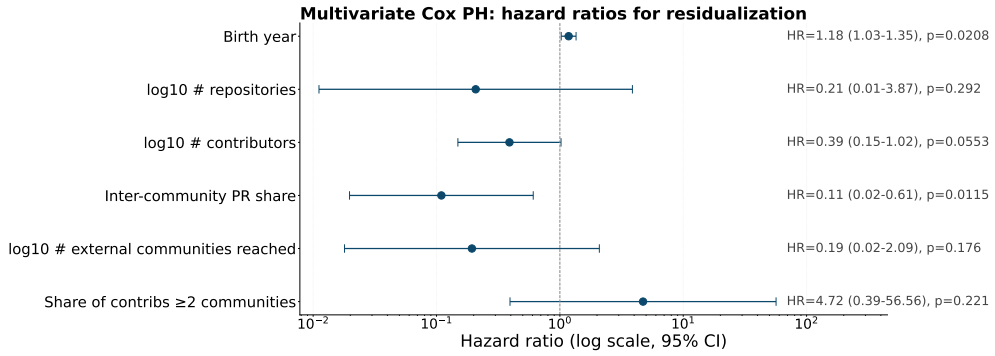


Fig. S12 Predictors of community residualisation hazard: multivariate Cox proportional-hazards forest plot. $n = 163$ communities, 55 events; concordance $C = 0.843$. Hazard ratios on a logarithmic axis with 95% Wald confidence intervals; the dashed vertical line is $HR = 1$. After controlling for cohort [birth year] and size [\log_{10} # repositories, \log_{10} # contributors], the inter-community PR share is significantly protective [$HR = 0.11$, 95% CI [0.02, 0.61], $p = 0.012$]; birth year retains an independent unfavourable effect [$HR = 1.18$ per year, $p = 0.021$]; \log_{10} # contributors is borderline [$p = 0.055$]. The same numbers are reported as Table 1 in the main text; the corresponding Kaplan–Meier stratifications by inter-community PR share and external-community degree are panels B and C of Figure 4.

S.8 Boundary friction and collaboration depth

This section supports the boundary-friction analysis in the main text (Figure 5) by stratifying the per-PR friction indicators by the author’s commit-level breadth k .

S.8.1 How boundary friction varies with contributor breadth k

The four boundary-friction indicators reported in the main text (Figure 5) compare intra- versus inter-community pull-requests and issues but pool every author together. A natural follow-up question is whether the friction is borne uniformly across contributors or is instead concentrated in a particular layer. We answer this by linking

each pull-request to its author’s commit-level breadth k [the number of distinct Louvain communities that author has committed to in the corpus] and re-tabulating Figure 5A–B by k -bin.

Identity reconciliation.

The commit metadata in our primary stream uses `author_uniqueID`, which is in 86.9% of rows a numeric GitHub user identifier and in the remainder a login string; the GitHub Archive event stream and the per-PR review-depth table use login strings throughout. To align the two we built an `actor_id` \leftrightarrow `actor_login` map from the GitHub Archive [one row per event, 490,990 unique `actor_ids`, 507,395 unique logins] and re-keyed every commit row by the resulting canonical login. After canonicalisation the 11,370 raw `author_uniqueIDs` collapse to 11,189 canonical contributors. Of these, eleven are explicit bots [`[bot]` suffix or known automation accounts: `dependabot[bot]`, `dependabot-preview[bot]`, `renovate[bot]`, `github-actions[bot]`, `allcontributors[bot]`, `deepsource-autofix[bot]`, `imgbot[bot]`, `mergify[bot]`, `pre-commit-ci[bot]`, `whitesource-bolt-for-github[bot]`, plus `gitter-badger`] and 688 are phantom git identities – numeric identifiers that do not resolve to a GitHub login in our window [these reflect committers whose authorship metadata never matches a recorded GitHub account, e.g. legacy or deleted accounts] plus the generic `root/admin/git/user` placeholders. Both classes are excluded throughout the cross-community contributor analysis because their k counts conflate multiple humans [default git server identities] or reflect automation rather than human boundary-spanning. After filtering, the canonical human cross-community contributor layer at the data-driven boundary $k \geq 7$ comprises nine humans, of which the four with $k \geq 10$ are `noraj`, `cclauss`, `Oxflotus`, and `timgates42`. The two automated $k \geq 10$ identifiers that the unfiltered count would have included are `dependabot[bot]` [a dependency-update bot that authored 7,917 pull requests in the corpus] and `gitter-badger`; the two phantom $k \geq 10$ identifiers are the placeholder logins `root` [$k = 20$] and `148100` [$k = 31$]. Removing the bot subset alone subtracts $\sim 24\%$ of the unfiltered 5,612 inter-community merged pull requests [`dependabot[bot]` contribution] and is the single largest correction induced by the procedure.

Per-PR friction by author k .

Linking the per-PR review-depth table to the canonical k assignment gives 56,356 pull requests with a resolved [non-bot, non-phantom] author. Splitting these by intra/inter and by author’s k -bin yields the patterns in Figure S13.

For *intra-community* pull-requests, acceptance is roughly flat at 78–92% across all k -bins, and median turnaround sits between 10 and 60 hours – the small variation is consistent with the per-bin sample sizes shrinking from 37,361 at $k = 1$ to 69 at $k \geq 10$.

For *inter-community* pull-requests the friction varies dramatically with the author’s k . Acceptance rises monotonically from 42.3% at $k = 1$ [$n = 376$] to 76.1% at $k = 2$ [$n = 737$], 71.7% at $k = 3$ –4 [$n = 569$], and 86.7% at the $k = 5$ –9 bin [$n = 556$]. Median turnaround on inter-community pull-requests collapses by a factor of ~ 3 , from 147.4 hours at $k = 1$ to 48.9 hours at $k = 5$ –9 – essentially indistinguishable from

the intra-community median there. The CHANGES_REQUESTED rate also drops from 2.4% at $k = 1$ to 0.7% at $k = 5-9$. The five humans at $k \geq 10$ [$n = 172$ inter-community PRs] sit between the $k = 5-9$ bin and $k = 2$ contributors on acceptance [61%] and median turnaround [66 hours], with a wide upper-quartile envelope that reflects a small sample dominated by a handful of recurring contributor-repository pairs.

Interpretation.

The boundary-friction gap reported as a single intra-vs-inter contrast in Figure 5 therefore over-states the friction faced by the cross-community contributor layer that does most of the cross-community work. High-breadth contributors at $k \geq 5$ submit inter-community pull-requests at the same speed and with the same acceptance odds as their intra-community ones; the residual friction in the corpus is concentrated in low- k submitters whose cross-community contribution is a one-off. This is consistent with a *recognition / repeat-relationship* mechanism: contributors with established cross-community presence have already accumulated the trust that low- k contributors must build during a single contested pull-request. The result also explains the asymmetry visible in panel-D of Figure 3: the same minority of repeatedly cross-committing contributors that produces the inter-community pull-request volume also faces little integration friction on those contributions, so the cross-community contributor layer absorbs cross-community work cheaply once trust is in place.

Per-PR friction (Figure~5) by contributor breadth k . Bots and phantom git identities filtered ($n_{\text{bot}}=11$, $n_{\text{phantom}}=688$).

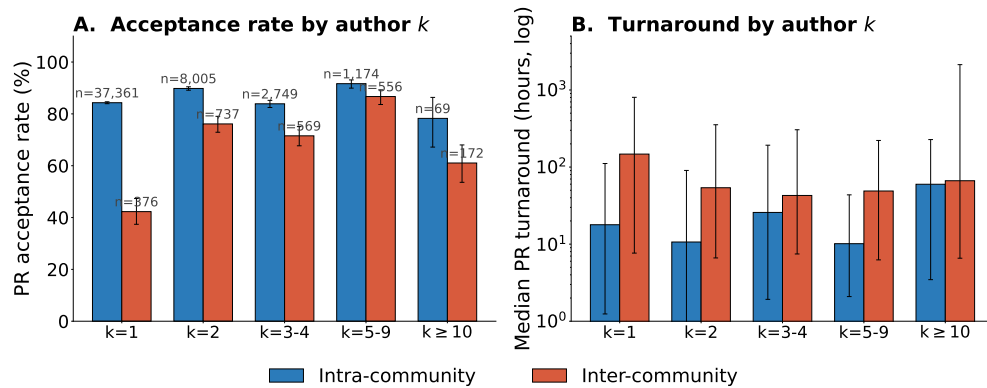


Fig. S13 Per-PR friction (Figure 5A–B) varies sharply with author breadth k . Pull requests are grouped by intra/inter [blue/red] and by their author’s commit-level k -bin after canonicalising contributor identity [author.uniqueID \rightarrow login via the GitHub Archive actor.id \leftrightarrow actor.login map] and removing 11 explicit bots and 688 phantom git identities. **A.** Acceptance rate [% of PRs ultimately merged] with Wilson 95% confidence intervals; per-bin sample sizes annotated above the bars. The intra-community curve is roughly flat at 78–92%, while the inter-community acceptance climbs from 42.3% at $k = 1$ to 86.7% at $k = 5-9$ and is 61% at $k \geq 10$ [$n = 172$]. **B.** Median turnaround [hours from PR open to terminal event] on a logarithmic axis; whiskers indicate the inter-quartile range. Inter-community turnaround at $k = 1$ is ~ 147 hours and falls to ~ 49 hours at $k = 5-9$ – a 3-fold compression that brings inter-community latency in line with intra-community latency. The boundary-friction gap reported in Figure 5A–B is therefore concentrated in low- k contributors; the cross-community contributor layer at $k \geq 5$ carries inter-community work at near-intra-community speed and acceptance.